

Dark Matter haloes as probes of modified gravity

Wojciech A. Hellwing,^{a,b,c} Steffen Knollmann,^d Alexander Knebe^d and Roman Juszkiewicz^{a,e}

^aInstitute of Astronomy, University of Zielona Góra, ul. Lubuska 2, 65-001 Zielona Góra, Poland

^bInterdisciplinary Center for Mathematical and Computational Modeling, University of Warsaw, ul. Pawińskiego 5a, 02-106 Warsaw, Poland

^cInstitute for Computational Cosmology, Department of Physics, Durham University, Science Laboratories, South Rd, Durham DH1 3LE, UK

^dGrupo de Astrofísica, Departamento de Física Teórica, Módulo C-8, Facultad de Ciencias, Universidad Autónoma de Madrid, 28049 Cantoblanco, Madrid, Spain

^eNicolaus Copernicus Astronomical Center, ul. Bartycka 18, 00-716 Warsaw, Poland

E-mail: pchela@icm.edu.pl

Abstract. We investigate the effect of hypothetical long-range scalar interactions present in the Dark Matter sector on to the internal properties of Dark Matter haloes. We employ a particular formulation of such modified cosmology called the ReBEL model, in which the additional interactions between Dark Matter particles are modeled on a phenomenological level as modification of the gravity. We perform a series of high resolution cosmological N-body simulations of 512^3 particles for five different ReBEL models and for one reference Λ CDM model. We compare density profiles, velocity curves, the spin and shape parameters (triaxiality and ellipcities) between models using statistical distributions of these quantities as well as direct comparison of haloes cross-correlated between the ReBEL and the Λ CDM models. We also test and compare the state of the virialisation of the haloes in our models. We find that statistically the ReBEL halo density profiles are also described quite well by the Navarro-Frenk-White profile, but we denote an increase of the mean virial concentration parameter by 6% to 15% for our range of tested ReBEL models. We also find that the velocity curves for our modified gravity haloes reach their maxima at smaller radii when compared to standard cosmology haloes. We also denote a slight increase of the mean of the halo spin parameter reflecting a bit higher rotational support of the haloes due to the scalar interacting Dark Matter. On the other hand we do not find any significant differences in shapes of the haloes between standard and modified gravity paradigms. Finally we report that in the class of modified Dark Matter models we study here the overall virialisation state of DM halo is higher compared to the Λ CDM haloes. The cosmological implications and prospects for using haloes as probes of modified gravity is briefly discussed.

Keywords: cosmology, dark matter, haloes, large-scale structure, phenomenology

ArXiv ePrint: [not yet](http://arxiv.org/abs/1111.7257)

Contents

1	Introduction	1
2	Scalar-interacting DM: The ReBEL model	3
2.1	The phenomenological model & modified gravity	5
2.2	The growth of structures in the ReBEL model	6
3	N-body simulations	7
4	Results: Statistical properties of the halo populations	10
4.1	Density profiles & rotation curves	10
4.2	Spin & halo rotation	14
4.3	Shapes and geometry	18
4.4	Virialisation	21
5	Results: Properties of cross-correlated haloes	25
5.1	The virial mass	25
5.2	The triaxiality parameter	26
5.3	The spin parameter	27
5.4	The concentrations	27
6	Conclusions	28

1 Introduction

The Λ cold dark matter (Λ CDM) model has proven to be capable of explaining a tremendous amount of observational data. As we entered the era of precision cosmology — both observationally and from a modellers perspective — we are left with a more and more detailed picture of what actually took place when the Universe cooled down and formed structures starting from $z \sim 1100$ to the present day.

The strong relationship between dark matter characteristics and the emerging large scale structure has already been investigated in large detail. Nonetheless, while most of the attention has focused on very large scale linear structures or the properties of highly non-linear small-scale objects like haloes of galaxies, there remains a considerable amount of questions with respect to the physical nature of the Dark Matter. Taking into account all the difficulties linked with the direct detection of a dark matter particle showing up in Earth-based experiments, like the Large Hadron Collider at CERN, astrophysical observations still form, by far, the most important source of information on the physical properties and nature of the mysterious dark matter. Within this context, one of the important questions concern a number of unresolved problems of the well established paradigm of cold dark matter (CDM). These concern galaxy scale riddles such as the precise quantitative understanding of the rotation of galaxies, the central cusp of dark matter haloes and the problem of reconciling the observed rich population of thin disk dominated spiral galaxies with the LCDM implied high merger and accretion rate at low redshifts (for an excellent discussion refer to [1, 2]).

Perhaps the most interesting challenge for the concordance Λ CDM cosmology is the well-known void phenomenon, strongly emphasised by P.J.E. Peebles [3]. It concerns the apparent discrepancy between the number of observed dwarf halos in cosmic voids and that expected from CDM simulations.

Some of the scientists could call this array of unresolved problems a “galaxy formation crisis”, others would not probably go as far as to call this situation a crisis. Nevertheless how we decide to call this situation, we are forced to admit that there are noticeable tensions between what observations suggest and what (cosmological simulations of) the Λ CDM model seems to predict. This series of unresolved issues related to the galaxy formation paradigm rendered with the CDM part of the Λ CDM model encouraged some researchers to look for a sensible alternative or a modification of the CDM paradigm. Studies of possible exotic new physics of the Dark Matter are also very important from a high-energy physics point of view. Possible falsification of some of the modified DM models will narrow down the number of allowed DM particle candidates.

One of such a possible CDM paradigm modification formulated on the grounds of supersymmetry and string theory has been found and developed by Gubser, Peebles and Farrar. It consists of cold dark matter that is additionally (to usual gravity) interacting by means of an exchange of scalar particles. This model was dubbed the ReBEL (*daRk Breaking Equivalence principLe*) and discussed in recent years in the literature [4–7]. These studies have shown that the model has the potential to alleviate some tensions and to help the theoretical Λ CDM model to possibly overcome the difficulties at the scales important to galaxy formation. The ReBEL model is a slight modification to the standard cold dark matter model. In its core the model introduces an additional interaction between the DM particles, a so-called “fifth force”, which acts exclusively on DM only and has a limited range. Studies employing N-body simulations of the ReBEL model [1, 8–13] and similar models of coupled DM and DE [14, 15] have shown that this class of models have the ability to explain observed properties of the large-scale structure of the Universe (like 1D power spectrum of Ly- α forest galaxies or the power spectrum from the SDSS galaxy survey¹) as well as the Λ CDM model does. At the same time, it was shown that the ReBEL model can introduce interesting and potentially positive effects to the process of structure formation on galactic scales.

In the recent years models invoking on of another from of modified or exotic DM physics, including models of coupled DM and DE, has been studied in many works [16–26]. On the other hand we also seen recently reports of yet another observations possibly posing challenge for the standard CDM paradigm, these include observed offset between baryonic and DM in clusters [27], reports on supermassive superclusters observed at high redshifts [28–30] and its implications for the Λ CDM and coupled DM-DE theories [31–33]. This taken together clearly indicates that the very physical nature of DM is currently hotly discussed and debated topic. In this paper we study the impact of the ReBEL model and its form of modified gravity on internal properties of DM haloes. Therefore this work hopefully will add to the international and multidisciplinary collective effort taken to further understand and study the nature of DM and its implication for cosmology.

This paper is organised as follows: in §2 we layout in details the theoretical formulation and the physics of the ReBEL model; in §3 we describe the numerical experiments we performed to study DM haloes; the sections §4 §5 cover the presentation and discussion of our results; finally in the §6 we give our conclusions and final remarks.

¹Sloan Digital Sky Survey - <http://www.sdss.org/>

2 Scalar-interacting DM: The ReBEL model

Now we will briefly recapture after other authors [4, 5, 8], the fundamental ideas and properties of the model discussed in this paper.

We consider the picture in which there exist a long-range force - different than gravity - that acts upon only dark matter. Such force can be exerted due to the interactions between DM particles and some underlying background scalar field ϕ . Elementary action integral for such dark matter will have the following form:

$$\mathcal{S} = - \int |\phi| ds, \quad \text{or} \quad (2.1)$$

$$\mathcal{S} = \int \sqrt{-g} d^4x (i\bar{\psi}\gamma\partial\psi - \phi\bar{\psi}\psi). \quad (2.2)$$

The idea of the long-range interactions appearing due to exchange of massless scalar particles has very long history. Nordström derived the classical form of (2.1) already in 1913 [34]. This interaction is equivalent to the form (2.2) introduced by Yukawa [35], if the appropriate de Broglie lengths are small.

In the framework of the quantum field theory (QFT) we can find important arguments stating that it is very unlikely for any scalar field to escape from obtaining large mass ($\gg H_0$), which would make any model with a scalar field particularly useless for cosmology. However some work on the grounds of the string theory suggest that there is a possibility for a scalar field to maintain low mass.

In the beginning of the second half of the 20th century Pascual Jordan and Robert Dicke presented a few papers exploring the physics of the scalar-tensor gravity implementing above action integral and defined for particles in the Einstein frame [36–38].

In 1990 Damour *et al.*[39] noticed that the tight empirical constrains that we have for long-range scalar interactions in the baryon sector allow for existence of such interaction with significant strength in the dark sector.

Modern considerations along this line of thought appear abundantly in the literature of this subject [40–52].

We will focus now on the model described in details by Gubser, Peebles [4, 5]. Let's consider at least two different species of dark matter particles interacting, in addition to gravity, by the scalar field. This additional interaction is dynamically screened by the presence of light particles coupled by Yukawa-like factor to the scalar field. The generic Lagrangian for such Dark Matter will be:

$$\begin{aligned} \mathcal{L} = & \frac{1}{2}(\partial\phi)^2 + \bar{\Psi}_s i\bar{\nabla}\Psi_s + \bar{\Psi}_+ i\bar{\nabla}\Psi_+ \\ & + \bar{\Psi}_- i\bar{\nabla}\Psi_- - y_s \phi \bar{\Psi}_s \Psi_s - (m_+ + y_+ \phi) \bar{\Psi}_+ \Psi_+ - (m_- - y_- \phi) \bar{\Psi}_- \Psi_-, \end{aligned} \quad (2.3)$$

where $\bar{\nabla}$ is the operator in Feynman slashed notation.

$$\mathcal{A} \equiv \gamma^\mu A_\mu. \quad (2.4)$$

Here γ^μ are Dirac's gamma matrices and the equation is written in the Einstein summation convention. The constants m_\pm and y_\pm are positive. The fermions Ψ_\pm are non-relativistic Dark Matter and the additional species of light particles Ψ_s consist of the screening particles.

The action for the two species of dark matter will assume the form:

$$\mathcal{S} = \int \sqrt{-g} d^4x \phi_{,i} \phi^{,i} / 2 - \sum_{\text{particles}} \int [m_+(\phi) ds_+ + m_-(\phi) ds_-], \quad (2.5)$$

where the subscript $, i$ marks a partial derivative. The Dark matter particles now will carry effective scalar charges Q :

$$Q_+ \equiv \frac{dm_+}{d\phi} < 0, \quad Q_- \equiv \frac{dm_-}{d\phi} > 0, \quad \frac{d^2m_\pm}{d^2\phi} \geq 0, \quad (2.6)$$

which in general are conserved for non-relativistic phenomena². The field ϕ will undergo quasistatic relaxation towards equilibrium, yielding larger values in the regions where the (+) particles dominate and smaller values in aggregations of the (-) particles. Thus a particle with positive (+) charge will be attracted towards regions where the ϕ is large to reduce its energy $m_+(\phi)$, and adequately negatively charged particle (-) will move in the opposite direction also to reduce its energy. This behaviour implies that the particles of the same kind (charge) will attract each other and the particles of different kinds will repel.

We further assume that we will have two species of the Dark Matter particles which satisfy:

$$m_{DM} = m - y\phi, \quad m_s = y_s\phi, \quad \text{and } y\bar{n} < y_s\bar{n}_s \quad (2.7)$$

where m_{DM} is the mass of heavy particle species (effectively the mass of a DM particle), m_s labels the mass of the screening particles and \bar{n} & \bar{n}_s are the corresponding number densities of this particles. The scalar field ϕ has relaxed to quasistatic equilibrium, for which $m_s \sim 0$. Thus the screening particles will be relativistic and will generate the potential:

$$V_s = \sum_{\text{particles}} \int y_s \phi ds \simeq \int d^4r y_s \phi n_s \langle \sqrt{1 - v^2} \rangle. \quad (2.8)$$

We will have as well:

$$\frac{\delta V_s}{\delta \phi} = y_s n_s \langle \sqrt{1 - v^2} \rangle \simeq \frac{y_s^2 \bar{n}_s}{\varepsilon_s} \phi, \quad \text{where: } \varepsilon_s = \frac{y_s \phi}{\sqrt{1 - v^2}}. \quad (2.9)$$

Here the ε_s labels the averaged energy of a screening particle and $\langle \sqrt{1 - v^2} \rangle$ is the mean velocity of the screening particles (when $c = 1$). The equation for the scalar field will assume now the form:

$$\nabla^2 \phi = \frac{\phi y_s^2 \bar{n}_s}{\varepsilon_s} - y n(\mathbf{r}, t). \quad (2.10)$$

We can define the term that is effectively dumping the scalar field ϕ :

$$r_s = \sqrt{\frac{\varepsilon_s}{y_s^2 \bar{n}_s}} \quad [\text{Mpc}], \quad (2.11)$$

and we will dub it as **the screening length**³. Now we can rewrite the scalar field equation to the new form:

$$\nabla^2 \phi = \frac{\phi}{r_s^2} - y n(\mathbf{r}, t). \quad (2.12)$$

Here the last term describes the non-relativistic particles in a hydrodynamic approximation. The term ϕ/r_s^2 appears here, because the source term of the ϕ field for a particle with velocity v contains factor $ds/dt = \sqrt{1 - v^2}$ and for quasistatic configurations of the ϕ the energy of the screening particles

²In case of the interactions with relativistic energies the scalar charges are not conserved. Additionally, the scalar charge of DM trapped in a black hole is lost.

³This term is equivalent to the cut-off length in a Yukawa-like potential

ε_s (see Eqn. (2.9)) is nearly independent of their location. Elimination of the $\sqrt{1 - v^2}$ factor from ε_s leads to the equation for the screening length (2.11). The ε_s energy does not depend on time (it is constant), thus due to the expansion of the Universe it has to scale like $\varepsilon_s \propto a(t)^{-1}$. If we now denote that $n_s \sim a(t)^{-3}$ then we will arrive at the conclusion the the screening length will grow like $r_s \sim a(t)$. Hence it will be constant in a comoving frame.

The scalar field generated by a single DM particle will have the value of $\phi = y/4\pi r$ at the distance $r \ll r_s$. The force exerted by this field on another DM particle equals to the negative gradient of the mass $m - y\phi$. Ergo:

$$\mathbf{F}_s = y\nabla\phi. \quad (2.13)$$

This clearly shows that the two DM particles will be attracted by the scalar interaction:

$$F = \frac{y^2}{4\pi r^2} \quad \text{for } r \ll r_s. \quad (2.14)$$

Two DM particles interact also gravitationally and this allows us to define a parameter which will be a measure of the ratio of the scalar to gravitational force strength between two identical DM particles. We define such parameter as:

$$\beta = \frac{y^2}{4\pi G m^2}. \quad (2.15)$$

Setting $\beta \sim \mathcal{O}(1)$ will give us the scalar interactions whose magnitude for $r \ll r_s$ is comparable to the strength of the gravity. For distances much larger than the screening length this scalar interactions will fade away to zero. Hence the formula for the total force exerted on two DM particles can be splitted into two special cases:

$$F_{DM} = (1 + \beta)F_N \quad \text{for } r \ll r_s, \quad (2.16)$$

$$F_{DM} = F_N \quad \text{for } r \gg r_s. \quad (2.17)$$

To summarise : we are dealing with the model of the Dark Matter which additionally interacts by means of the scalar field. The model introduces two free parameters β and r_s , which in the phenomenological sense are sufficient to its full description.

2.1 The phenomenological model & modified gravity

Following the earlier work of [8, 9] in this paper we will study the ReBEL model using its phenomenological parametrisation. In this approach we will model the scalar interactions appearing in the dark sector as effectively **modified gravity** on the scales of interest. The modified potential between two DM particles will assume the form:

$$\Phi(\mathbf{r}) = -\frac{Gm}{r}h(r) = \Phi_N h(r), \quad (2.18)$$

where

$$h(r) = 1 + \beta e^{-r/r_s}. \quad (2.19)$$

Here G is the Newton gravitational constant, \mathbf{r} marks the separation vector between particles and Φ_N is the pure Newtonian potential. As we described in the previous paragraph our model is described by two parameters: β - the dimensionless factor measuring the ratio between the scalar and gravitational forces and r_s - the screening length expressed in Mpc. The elementary considerations from the string theory [4, 5, 8] give crude estimations of the order of magnitude of this parameters to be:

$$\beta \sim \mathcal{O}(1), \quad r_s \sim 1\text{Mpc}. \quad (2.20)$$

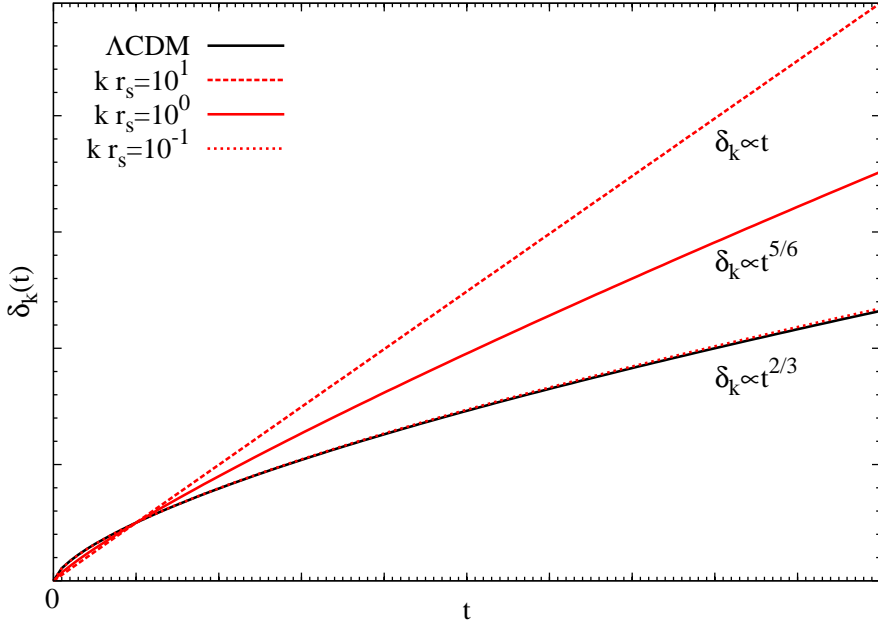


Figure 1. Growth of the Fourier modes of density perturbations in the linear regime during the matter-domination era as predicted by the equation 2.25. Solid black line depicts the Λ CDM model with $\delta_k \propto t^{2/3}$ for all values of k . Solid, dotted and dashed red lines mark the growth of the δ_k in the ReBEL model with $\beta = 1$ and q the three different values of $r_s \cdot k$. Both axes have arbitrary units.

The potential (2.18) gives rise to modified force-law between two DM particles:

$$F_{DM} = -G \frac{m^2}{r^2} \left[1 + \beta \left(1 + \frac{r}{r_s} \right) e^{-\frac{r}{r_s}} \right] = F_N \cdot F_s(\beta, \gamma), \quad (2.21)$$

$$\text{where: } \gamma \equiv \frac{r}{r_s}, \quad F_s(\beta, \gamma) = 1 + \beta(1 + \gamma)e^{-\gamma}. \quad (2.22)$$

Here the term F_s measures the force deviations from the usual Newtonian gravity and the F_N marks the Newtonian force. We will call F_s the ReBEL factor. For $\beta = 0$ or $\gamma \gg 1$ we will get $F_s \rightarrow 1$, hence $F_{DM} \rightarrow F_N$ and we recover the standard Newton force law.

Equations (2.18)-(2.22) yield a simple phenomenological description of the ReBEL addition to the CDM model.

2.2 The growth of structures in the ReBEL model

Having defined our phenomenological approximation to the ReBEL DM physics (equations 2.18-2.21) we can look more into the details of how the scalar forces affect the structure formation during the matter-dominated epoch. We can study this using linear perturbation theory (LPT) for the regime $\delta \lesssim 1$. Because the studied model change the dynamics of the DM only on scales small compared to the Hubble scale, it will not affect the global evolution of the scale factor described by the Friedman equations. Taking into account modified force law and modified Newtonian potential of the ReBEL model we can rewrite the Poisson equation to a new ReBEL form (only for DM component):

$$\vec{\nabla} \times \Phi = 0, \quad \nabla_{\vec{r}}^2 \Phi = 4\pi G \rho \left(1 + \beta e^{-|\vec{r}|/r_s} \right). \quad (2.23)$$

Linearising this equation together with the Euler and continuity equation with respect to small perturbations in δ , v_p and ϕ (the density, velocity and gravitational potential perturbations around smooth background) [53] we can obtain density perturbation evolution equation for Einstein-de Sitter Universe with $\Omega = 1$ (which we write in the Fourier space for convenience):

$$\ddot{\delta}_k + \frac{4}{3t} \dot{\delta}_k = \frac{2}{3t^2} \left[1 + \frac{\beta}{1 + (kr_s)^{-2}} \right] \delta_k. \quad (2.24)$$

The growing mode solution for this equation is [8]

$$\delta_k \propto t^\alpha, \quad \alpha = \frac{1}{6} \sqrt{25 + \frac{24\beta}{1 + (kr_s)^{-2}}} - \frac{1}{6}. \quad (2.25)$$

For $kr_s \ll 1$ we will get $\alpha = 2/3$, thus Fourier mods with $k \ll r_s^{-1}$ will grow exactly in the same manner like in the standard Cold Dark Matter model. On the other hand perturbations on scales smaller than characteristic screening length ($k \gg r_s^{-1}$) will grow faster than in standard model, in particular case for $\beta = 1$ we will have $\delta_k \propto t$. To depict explicit differences in the time evolution of some Fourier density mods in the LCDM and the ReBEL model we show the Fig. 1. In this figure we plot the time evolution of the ReBEL δ_k for three modes satisfying $kr_s = 10, 1, 0.1$, also for comparison we plot standard result for the LCDM case. As expected we denote that structure formation in the ReBEL model is enhanced and accelerated in compare to the LCDM case on scales $\leq r_s$. Moreover in this picture the Fourier modes experience different time evolution: from $\delta_k \propto t$ for $kr_s \ll 1$ to $\delta_k \propto t^{2/3}$ for $kr_s \gg 1$. Faster growth of the small-scale density perturbations in the ReBEL model will make this modes to cross non-linear regime ($\delta \gg 1$) quicker, which should result in earlier DM haloes formation and virialisation. This was already shown to some extent in [1, 11].

3 N-body simulations

Table 1. The parameters describing our N-body simulations. The β and r_s [h^{-1} kpc] depict the values of the ReBEL model free parameters used in a given simulation run, L is the box size (expressed in h^{-1} Mpc), z_{ic} is the redshift of the initial conditions, Ω_m and Ω_Λ are the dimensionless density parameters (for $z = 0$) for the dark matter and dark energy respectively, σ_8 is the r.m.s. of the density fluctuations smoothed at $R = 8h^{-1}$ Mpc, h is the dimensionless Hubble parameter, m_p is the mass of a single DM particle divided by $10^8 h^{-1} M_\odot$, ε render the force resolution (in h^{-1} kpc) and eventually by l we have labelled the mean inter-particle separation (in h^{-1} kpc).

Simulation	β	r_s	L	z_{ic}	Ω_m	Ω_Λ	σ_8	h	m_p	ε	l	N_p
LCDM	-	-	32	50	0.3	0.7	0.8	0.7	0.203	6	62.5	512 ³
B05RS100	0.5	100	32	50	0.3	0.7	0.8	0.7	0.203	6	62.5	512 ³
B05RS200	0.5	200	32	50	0.3	0.7	0.8	0.7	0.203	6	62.5	512 ³
B05RS500	0.5	500	32	50	0.3	0.7	0.8	0.7	0.203	6	62.5	512 ³
B05RS1000	0.5	1000	32	50	0.3	0.7	0.8	0.7	0.203	6	62.5	512 ³
B1RS1000	1.0	1000	32	50	0.3	0.7	0.8	0.7	0.203	6	62.5	512 ³

As mentioned earlier previous considerations in the literature of the subject provide a crude estimate of the values of the free parameters to be of orders $\beta \sim 1$ and $r_s \sim 1h^{-1}$ Mpc [8, 9]. In this paper we explore two possible values of the $\beta = 0.5, 1$ and four values of the screening length parameter $r_s = 0.1, 0.2, 0.5, 1h^{-1}$ Mpc. We label the corresponding simulations runs as LCDM, B05RS01, B05RS02, B05RS05, B05RS1, B1RS1, where b stands for β and rs marks the r_s parameter. In the LCDM run we use $\beta = 0$ (i.e. no scalar forces). To follow the formation of structures

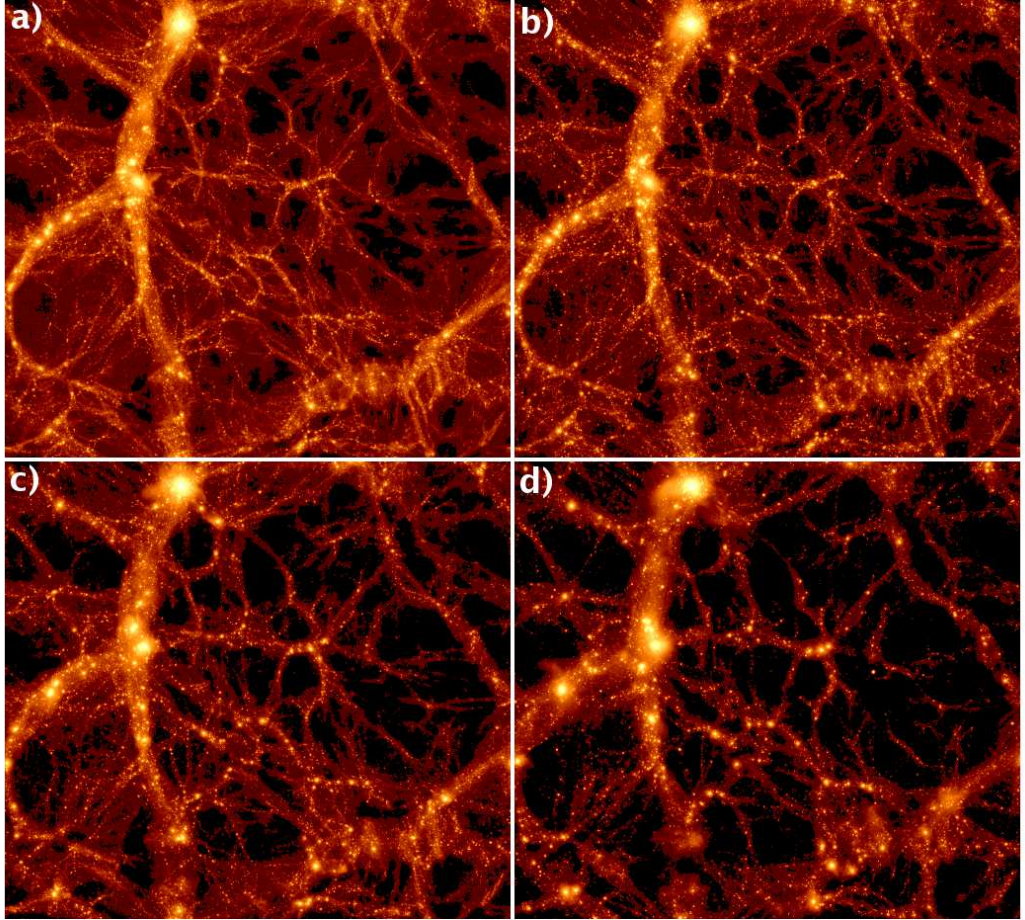


Figure 2. Comparison of the $z = 0$ density slices for four out of six considered models. The panels show the DM density in slices $32 \times 32 \times 3.2 h^{-1}$ Mpc. The labels depict as follows: a) the LCDM run, b) the B05RS200 run, c) the B05RS1000 and d) stands for the B1RS1000 model.

within the ReBEL framework we use an adapted version of the GADGET2 code [54]. For the detailed descriptions of the modifications made to the code we refer the reader to our previous paper on this subject [9]. We have conducted a series of high-resolutions DM only N -body simulations containing 512^3 particles within periodic box of $32h^{-1}$ Mpc comoving side length. The cosmology used in the simulations was the canonical Λ CDM with $\Omega_m = 0.3$, $\Omega_\Lambda = 0.7$, $\sigma_8 = 0.8$ and $h = 0.7$. Thus our mass resolution is $m_p \simeq 2.033 \times 10^7 h^{-1} M_\odot$. The force softening parameter was set to be $\varepsilon = 6h^{-1}$ kpc. All simulations were started with the same initial conditions at $z_{ic} = 50$, and varied only in the ReBEL parameters. For each run we saved 30 snapshot equally spaced in the logarithmic time scale starting from $z = 6.092$ to $z = 0$. We give the parameters of our simulations in the Tab. 1.

We used the MPI+OpenMP hybrid AMIGA halo finder (AHF) to identify haloes and subhaloes in our simulation⁴. AHF is the successor of the MHF halo finder by [55], a detailed description of AHF is given in the code paper [56]. We note that we needed to adjust the code slightly to take the modified gravity of the ReBEL models into account. We have modified the unbinding procedure that removes from a given halo particles not bound by the potential energy of that halo, by applying the modified force and potential laws of the ReBEL model. Moreover the equation for a DM halo

⁴AHF is freely available from <http://popia.ft.uam.es/AMIGA>

circular velocity needs to be changed, since we have to take into account that DM particles, due to the presence of the scalar forces, have higher potential energies in the ReBEL model compared to the Λ CDM case. The revised proper equation for the circular velocity at distance R_{vir} in the ReBEL DM haloes has the form

$$V_c^{ReBEL} = \left[\frac{GM_{vir}}{R_{vir}} \cdot \left(1 + \beta(1 + R_{vir}/r_s)e^{-R_{vir}/r_s} \right) \right]^{1/2} = V_c \cdot (F_s(\beta, R_{vir}/r_s))^{1/2}, \quad (3.1)$$

where M_{vir} is DM mass inside R_{vir} , V_c is the circular velocity for the pure Newtonian dynamics and we have used the ReBEL factor from (2.22). This formula can be easily found by noting that on a circular orbit the centripetal force acting on a DM particle has an additional component coming from the scalar interactions.

Starting with the halo catalogues at $z = 0$ we construct the merger trees for each simulation by cross-correlating the particles constituting the haloes in consecutive time steps. For each halo we record all progenitors and select the main progenitor as the halo that maximises the merit function $N_1 N_2 / N_s^2$, where $N_{1,2}$ and N_s are the number of particles of the haloes and the number of shared particles, respectively. Throughout this paper we limit our analysis, if not explicitly stated otherwise, to DM haloes that contain at least 100 DM particles. Thus we set our minimal halo mass to $M_{min} = 2.03 \times 10^9 h^{-1} M_\odot$.

To summarise the description of our N-body simulations we present Fig. 2 where the reader can compare the differences in the density fields at $z = 0$ between four out of all our models. The panels show the DM density in slices cut from the whole computational box. The slices are $32 \times 32 \times 3.2 h^{-1}$ Mpc in dimension. For the weakest ReBEL model⁵ the density differences from the fiducial Λ CDM case can be small. Therefore – to obtain a fair ground for model comparison – we made use of a superior method for the actual density estimation: the Delaunay Tessellation Field Estimator (DTFE). The DTFE method was unfolded in a series of papers [57, 58] and recently Marius Cautun & Rien van de Weygaert kindly provided us with the public version of the DTFE code [59] that we have used for our density estimations. In Fig. 2 the averaged DTFE density contrast is now shown in a logarithmic colour space and for the comparison purpose the colour maps for each panel were normalised to the same scale. As we can see the structure and shape of the Cosmic Web (the large-scale pattern on clusters, filaments, walls and voids) is more or less preserved in the ReBEL runs when compared to the Λ CDM case. However, we can depict arising differences when looking into smaller scales. It appears that the stronger the scalar force the less small density clumps we see in the corresponding density slice. This property was confirmed to some extent by the shape and the amplitude of the ReBEL cumulative halo mass functions studied by Hellwing *et al.*[9, 11]. On the other hand we can also depict directly another striking feature of the ReBEL large-scale structures in the DM density field: It appears that the cosmic voids are more devoid of DM in the ReBEL case. This was already discussed in [8, 9]. From this brief analysis of the density slices we can already notice that the Megaparsec scale environment in which the DM haloes form can be, in general, different in both cosmologies, despite the same initial conditions. This fact potentially indicates that averaged internal properties of DM haloes can carry some markers of modified underlying force-law, and thus maybe provide a promising probe for modified gravity and fifth force theories. In the following section we will discuss our findings with respect to that matter.

⁵From now on as the weakest models we consider the ReBEL models with the lowest values of the free parameters β and r_s .

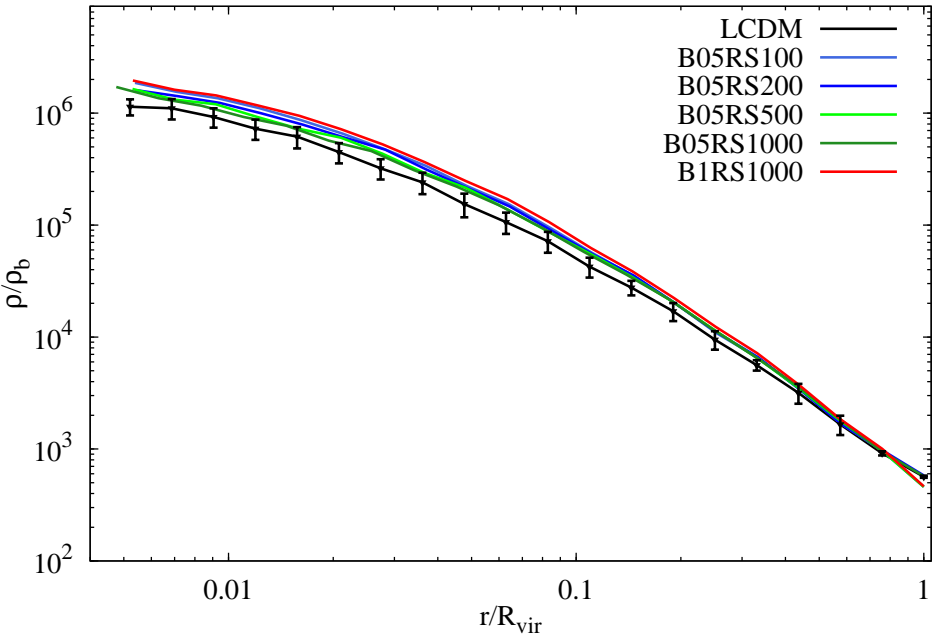


Figure 3. The comparison of the averaged density profiles of 10 Most Massive Haloes between all our ReBEL models and the fiducial LCDM run.

4 Results: Statistical properties of the halo populations

We start our analysis of various DM haloes' properties by comparing statistical distributions and statistical averages of their parameters. This will provide us with the information of how the presence of the long-range scalar interactions affect the whole population of DM haloes. We will further cross-correlate the halo-catalogues between the fiducial Λ CDM run and all inquired ReBEL models to investigate differences in the deduced individual halo properties. Studying these effect will give us insights on how the ReBEL cosmology inflicts and imprints on individual halo properties and histories.

4.1 Density profiles & rotation curves

Because in our model we change effectively the strength of the attractive forces of gravity on scales $r \leq r_s$, the most interesting question to ask first is probably the shape of the density profile for haloes in ReBEL cosmologies. We begin with comparing the averaged density profiles obtained by averaging over the 10 Most Massive Haloes (MMH10) found in each of our simulations. These haloes have mass in range of $2 \times 10^{13} M_\odot h^{-1} < M_{vir} \lesssim 10^{14} M_\odot h^{-1}$. We focus first on these most massive haloes since they have radii larger than $5 \times 10^2 h^{-1}$ kpc. This means that for models B05RS100, B05RS200 and B05RS500 these haloes are bigger than the fifth force screening length, whereas for models B05RS1000 and B1RS1000 the screening length is larger than haloes virial radii. Hence we can suspect that any significant deviations in the density runs induced due to existence of a new dynamical scale (the screening length), if present, should be imprinted in these very few most massive haloes. The comparison between averaged profiles is illustrated in Fig. 3. We can denote that in the inner parts of the MMH10 ($r < 0.1 R_{vir}$) the ReBEL haloes have higher density than the fiducial objects from the LCDM run. Thus we can expect that counterparts of the LCDM MMH10 will have higher concentrations. To asses this and further study the properties of the density profiles

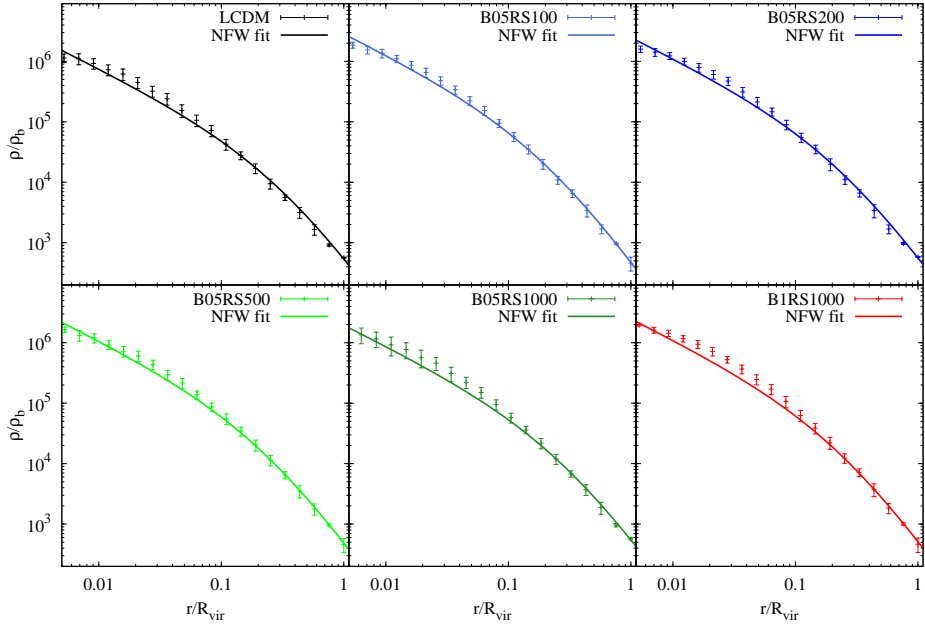


Figure 4. The MMH10 density profiles shown separately, together with the best NFW fits.

of the ReBEL haloes we will use the well known Navarro, Frenk & White (NFW) profile [60], which was proven to be universally good fit for the majority of Λ CDM DM haloes. The NFW profile is given as:

$$\rho_{NFW}(R) = \frac{\rho_0}{(R/R_s)(1 + R/R_s)^2}. \quad (4.1)$$

Here ρ_0 and R_s (not to be mistaken with r_s - the scalar force screening length parameter) are the parameters of the fit to be determined. The first parameter is the characteristic density and the second one is the scaling radius. The scaling radius is usually used to define the concentration parameter c_{vir} of a given NFW density profile:

$$R_{vir} = c_{vir} \cdot R_s, \quad (4.2)$$

where R_{vir} is the virial radius of a halo.

In Fig. 4 we now plot the MMH10 profiles together with the best NFW fits to them. Each panel shows the profile and the fit of the MMH10 form different simulation run. We can note that the NFW fit is reasonably good fit for all our MMH10 haloes. Thus we can conclude that a fifth force even with different screening lengths does not change the universality of CDM haloes density profiles reported Navarro, Frenk & White. Now we also compare the best-fit parameters for averaged profiles of the MMH10 that evolved in our different ReBEL models. The values are summarised in Tab. 2.

A brief study of the values shown in the table tells us that indeed the MMH10 in the ReBEL runs are characterised by higher characteristic densities and smaller scaling radii which in turn means lower virial concentration parameter. We can confirm such findings for all ReBEL MMH10s.

Now we turn to study the density profiles of all our DM haloes. We find that the NFW fit of the form (4.1) is also universally good fit for majority of haloes in the ReBEL runs. Using the NFW fit we have determined the R_s values for our haloes, thus we obtained the values of corresponding concentration parameters c_{vir} . We can use these values to further study the effect of the 'fifth' force onto the haloes density profiles in general. To evaluate that we show in Fig. 5 the distribution of the c_{vir} parameter for the haloes from the ReBEL run. In each case we also plot (black boxes) the

Table 2. The NFW best fit parameters for MMH10 density profiles.

Model	ρ_0	R_s/R_{vir}	c_{vir}
LCDM	21953	0.355463	2.813
B05RS01	58692.6	0.229483	4.358
B05RS02	41558.4	0.280253	3.568
B05RS05	43208.5	0.260596	3.837
B05RS1	28234	0.322564	3.100
B1RS1	43965.7	0.264509	3.780

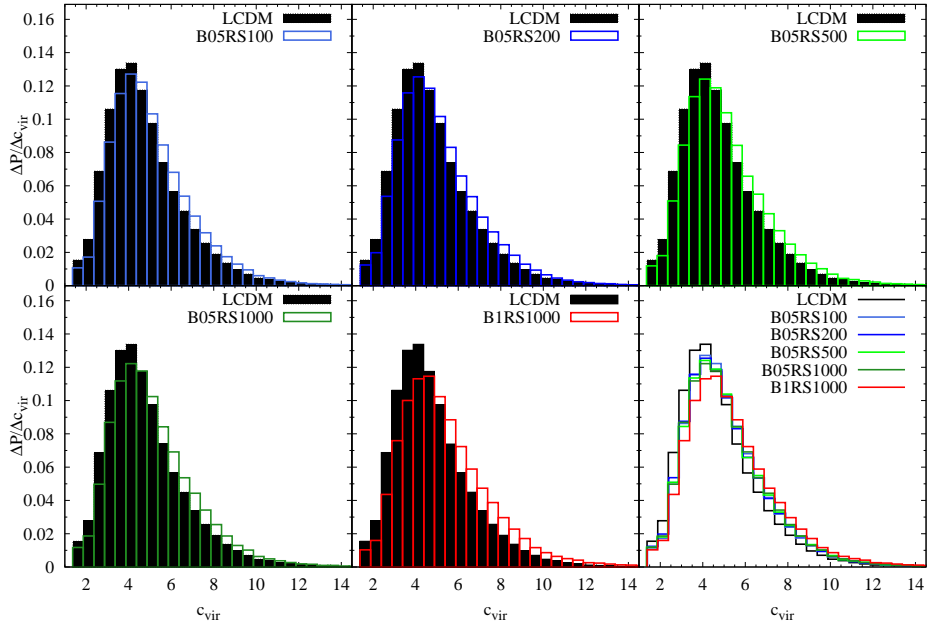


Figure 5. The distributions of the virial concentration parameter for our ReBEL models. In each panel we also plot for comparison the distribution of the Λ CDM case.

Table 3. The mean and the standard deviation for the c_{vir} distributions.

Model	\bar{c}_{vir}	$\sigma_{c_{vir}}$
LCDM	4.55	1.89
B05RS100	4.84	1.95
B05RS200	4.86	1.98
B05RS500	4.87	2.00
B05RS1000	4.89	2.01
B1RS1000	5.15	2.16

distribution obtained from the LCDM run which should be our fiducial case to compare with. The bottom-right panel presents distributions for all models taken together to allow for a direct comparison between all ReBEL models. Now we can clearly see that the ReBEL haloes are characterised by broader distributions with higher values of the mean c_{vir} parameter. Thus, on average, the ReBEL haloes have slightly higher concentrations. This effect, however, is not big as we can infer from the values listed in Tab. 3. The largest increase ($\sim 16\%$) in the mean of the concentration parameter

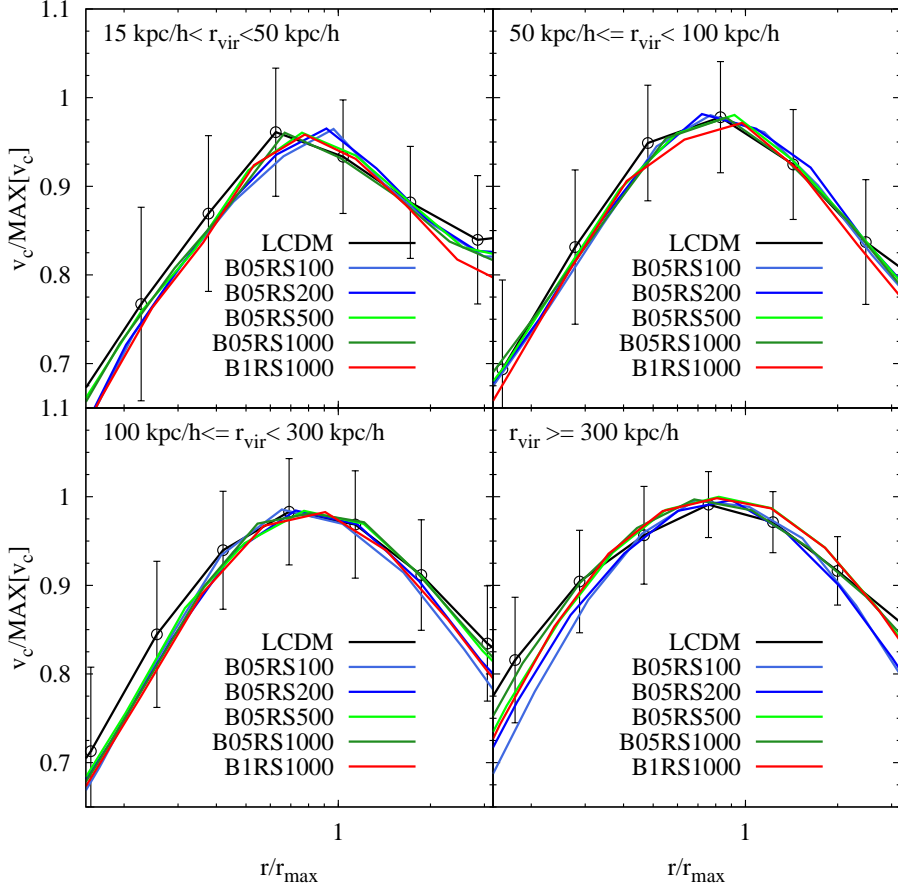


Figure 6. The averaged haloes circular velocities binned in radial bins. The four panels show data for four classes of haloes depending on their virial radius: $15h^{-1} \text{ kpc} \leq R_{vir} \leq 50h^{-1} \text{ kpc}$ (top-left), $50h^{-1} \text{ kpc} < R_{vir} \leq 100h^{-1} \text{ kpc}$ (top-right), $100h^{-1} \text{ kpc} < R_{vir} \leq 300h^{-1} \text{ kpc}$ (bottom-left) and $R_{vir} > 300h^{-1} \text{ kpc}$ (bottom-right). The curves were rescaled by the maximal v_{circ} value for each DM halo (see text for the details).

distribution can be noted for B1RS1000 model, while for the remaining ReBEL runs the increase is smaller and the effect is contained to $\lesssim 7\%$.

In Fig. 6 we now turn to the rotation curves showing the averaged circular velocity curves for haloes divided into four groups depending on their virial radii corresponding to virial mass ranges of $\sim 1.5 \times 10^{10} M_{\odot} h^{-1} \div \sim 4 \times 10^{10} M_{\odot} h^{-1}$, $\sim 4 \times 10^{10} M_{\odot} h^{-1} \div \sim 1.2 \times 10^{11} M_{\odot} h^{-1}$, $\sim 1.2 \times 10^{11} M_{\odot} h^{-1} \div \sim 3 \times 10^{12} M_{\odot} h^{-1}$ and $> 3 \times 10^{12} M_{\odot} h^{-1}$. The plots were obtained by first normalising the velocity curves for each particular halo by its maximal value ($MAX[v_c]$) and the value of the radius at which the curve reaches this maximum - r_{max} . Such a normalisation is removing the dependence of the rotation curve on the halo mass, thus allowing us to average the data in some specified halo mass range (or virial radius range, since both quantities are related to each other). In principle, the amount of impact made by the presence of the scalar forces on a given halo should also be sensitive to the value of the ratio R_{vir}/r_s (where r_s is the ReBEL screening scale and not to be confused with the scale-radius of the best-fit NFW profile). Haloes with R_{vir}/r_s much greater than unity should be less affected by the ReBEL forces than haloes whose virial radii are smaller than the considered screening length r_s . To visualise this (possible) effect in the analysis, we have divided all haloes into four groups depending on their viral radii: $15h^{-1} \text{ kpc} \leq R_{vir} \leq 50h^{-1} \text{ kpc}$ (top-left

panel), $50h^{-1} \text{ kpc} < R_{vir} \leq 100h^{-1} \text{ kpc}$ (top-right panel), $100h^{-1} \text{ kpc} < R_{vir} \leq 300h^{-1} \text{ kpc}$ (bottom-left panel) and $R_{vir} > 300h^{-1} \text{ kpc}$ (bottom-right panel). First we denote that the data scatter is much bigger than visible differences between the models. Thus in the statistical sense the rotation curves of haloes in the LCDM and the ReBEL models agree within 1σ scatter (only shown for Λ CDM for clarity). However we can also depict a systematic effect seen especially for larger haloes in the inner- and outermost inner parts of the velocity curves. It seems like the velocity curves for the ReBEL haloes drops quicker when we move outwards from the peak r_{max} value than the reference curve for Λ CDM. This is indicating that in the case of scalar interactions, the haloes reach their maximum of the rotation curve at smaller radii than in the normal gravity case. This is to be expected if we recall the result from the previous section indicating that the ReBEL DM haloes have more concentrated density profiles. What might be interesting to denote is that when we put aside the strongest ReBEL model for the moment (B1RS1000) and compare the curves for the ReBEL models with the same value of the strength parameter β , we observe interestingly that the largest effect of this systematical deviation from the fiducial case can be seen in the curves related to models with the smallest considered screening lengths (B05RS100 and B05RS200). This effect is best seen in the last two samples (bottom panels). This is very surprising as it contradicts our earlier statement that the amount of impact made by the scalar forces should be sensitive on the value of the ratio R_{vir}/r_s . Actually the effect shown in the velocity curves plots still supports this claim, however the data shows that the effect is anti-correlated with the value of the ratio. It seems that for circular velocities within a halo, the larger the ratio is (the bigger the difference between halo size and the screening length) the stronger it promotes the discrepancy between fiducial LCDM curves and the ReBEL models. We propose the following explanation of this phenomena. When the radius of a halo is smaller or comparable to the screening length of a given ReBEL model then inside that halo the gravity forces are enhanced but in the same manner throughout the whole halo. Therefore, for the $R_{vir}/r_s \leq 1$ gravity inside a halo is still scale-less. The picture changes when we deal with a halo whose radius is larger than the considered screening length ($R_{vir}/r_s > 1$). In that situation a characteristic scale at which the forces of gravity get effective enhancement appear within a halo and this scale is related directly to the screening length. Since most of the halo mass is concentrated in the inner parts (in dense cores or cusps) the presence of a short-range (compared to the halo radius) scalar forces makes these inner parts of the halo more bound compared to the case without scalar forces. Increasing the binding energy of the haloes' cores together with enhanced forces acting between particles makes the process of halo virialisation and transport of angular momentum towards the halo centre more effective. This clearly indicates that the presence of a characteristic length of gravity enhancement leaves its footprint in the distribution of a halo's circular velocity profile. Therefore, we conclude that if one wants to find a cleaner imprint of hypothetical scalar forces in the DM sector onto the internal halo properties, one should focus on DM haloes satisfying $R_{vir}/r_s < 1$. This should be an important pointer for future studies of the ReBEL model.

4.2 Spin & halo rotation

According to the tidal torque theory the angular momentum of a galaxy/DM halo is growing thanks to the gravitational tidal interactions between the DM proto-halo and the matter distribution surrounding it [61–66]. Thus we can express the angular momentum gained by the halo as

$$\mathbf{J}_i \propto \epsilon_{ijk} \mathbf{I}_{jl} \mathbf{T}_{lk}, \quad (4.3)$$

where \mathbf{I}_{jl} is the inertia tensor of the proto-halo and \mathbf{T}_{lk} is tidal torque tensor generated by the matter distribution in the vicinity of the halo. These tidal torque forces are also shaping characteristic web-like pattern of the matter large-scale structures, hence providing a connection between the angular

momenta of DM haloes and the matter distribution on Megaparsec scales. However, the late-time dynamical evolution imprints non-linear and gasodynamical effects that strongly erase primordial connection between matter distributions and angular momenta of DM haloes. In hierarchical structure formation scenarios the highly non-linear processes like tidal stripping, close encounters and major mergers will dominate the growth of the angular momentum at intermediate and small redshifts (see details in e.g. [67–71]). Nevertheless knowing that in the ReBEL class cosmologies attractive forces shaping the evolution of the DM are enhanced on Megaparsec scales, we can expect that these enhanced interactions caused by the presence of the scalar field could be somehow imprinted in the DM haloes’ angular momenta.

The spin parameter

The angular momentum of a DM halo is commonly parametrised by the dimensionless spin parameter [62]

$$\lambda = \frac{|J||E|^{1/2}}{GM^{5/2}}, \quad (4.4)$$

where E is the total mechanical energy of the halo, M is its mass, G is the Newton gravitational constant and J is the total angular momentum defined as

$$\mathbf{J} = \sum_i^N m_i \mathbf{r}_i \times (\mathbf{v}_i - \bar{\mathbf{v}}). \quad (4.5)$$

Here m_i is a mass of an i -th particle belonging to the halo, \mathbf{r}_i is a vector connecting the i -th particle with the halo centre, \mathbf{v}_i is a particle’s peculiar velocity and $\bar{\mathbf{v}}$ is the bulk velocity (averaged) of the halo mass centre. We adopt this dimensionless spin parameter, however, in the version proposed by [72] as our estimator of a DM halo angular momentum. We decided to use the Bullock *et al.* spin parameter parametrisation for our study. The Bullock spin parameter has the following form

$$\lambda = \frac{|j|}{\sqrt{2}R_{vir}V_c}, \quad (4.6)$$

where

$$V_c = \left(\frac{GM_{vir}}{R_{vir}} \right)^{1/2} \quad (4.7)$$

is the circular orbit velocity at R_{vir} and j is the specific angular momentum of the halo

$$j = \frac{1}{N_H} \sum_{i=0}^{N_H} \mathbf{r}_i \times \mathbf{v}_i. \quad (4.8)$$

Here the sum covers all particles belonging to a given DM halo $0 \leq i < N_H$. Equation (4.7) is correct for Newtonian gravity, but for haloes in the ReBEL simulations we have to use again the equation for the modified circular orbit velocity (3.1). The spin parameter defined as above measures DM halo rotational support. High values of the λ corresponds to haloes that are spinning fast, while a low λ is indicative of a slowly rotating halo. In Fig. 7 we show the distributions of the spin parameter for the DM halo catalogues from our simulations. At first sight we can identify a clear feature of the distributions computed for the ReBEL models, i.e. the centre of these are shifted towards higher λ values when compared to the fiducial LCDM spin distribution. This shift is accompanied by a broadening of the high spin tail of the distributions. Therefore we conclude that haloes in the ReBEL

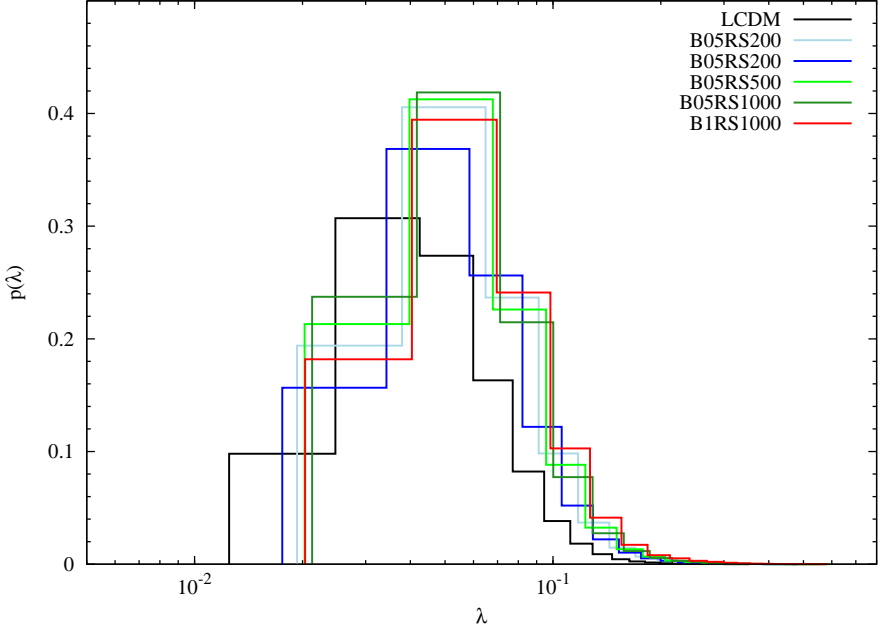


Figure 7. Distributions of the spin parameter for all considered models.

cosmologies have, in a statistical sense, higher spin values, thus are spinning faster than haloes in the Λ CDM case. We note that the largest deviations from the Λ CDM model appear for the strongest ReBEL models studied in this work, i.e. for B05RS1000 and B1RS1000. The shift of the centres of the spin distribution – however noticeable – does not appear to be large though. To check the statistical significance of this effect we will use the commonly accepted analytical model for the λ distribution: the distribution of the spin parameter of haloes in N-body simulations is well approximated by a log-normal function

$$p(\lambda)d\lambda = \frac{1}{\lambda\sigma\sqrt{2\pi}} \exp\left[-\frac{(\ln\lambda - \mu)^2}{2\sigma^2}\right] d\lambda, \quad (4.9)$$

with the centre of the distribution in the range $0.04 < \lambda < 0.05$ [73–77]. For the log-normal distribution the mean value (the expected value or the first moment) is given by

$$\lambda_0 = e^{\mu + \frac{1}{2}\sigma^2}, \quad (4.10)$$

and for the standard deviation we will have

$$\sigma_\lambda = e^{\mu + \frac{1}{2}\sigma^2} \sqrt{e^{\sigma^2} - 1}. \quad (4.11)$$

In Fig. 8 we now plot separately all the distributions of the λ parameter computed for all our halo catalogues accompanied with the best-fit log-normal functions of the form (4.9). In each panel we also list the values of λ_0 and σ_λ of the corresponding distribution. As can be seen the fitted log-normal functions describe quite well the underlying distributions for all models – even for the ReBEL models. For a better comparison of the derived parameters characterising the fitted distributions we collect them in Tab. 4. Taking together Fig. 8 and Tab. 4 we can denote that the expected value and the standard deviation of the fitted log-normal spin distributions are gradually increasing as we move from Λ CDM to the strongest ReBEL model B1RS1000. The maximum discrepancy in λ_0 appears between the Λ CDM model and the B1RS1000 and is over 30%. Although the increase of λ_0

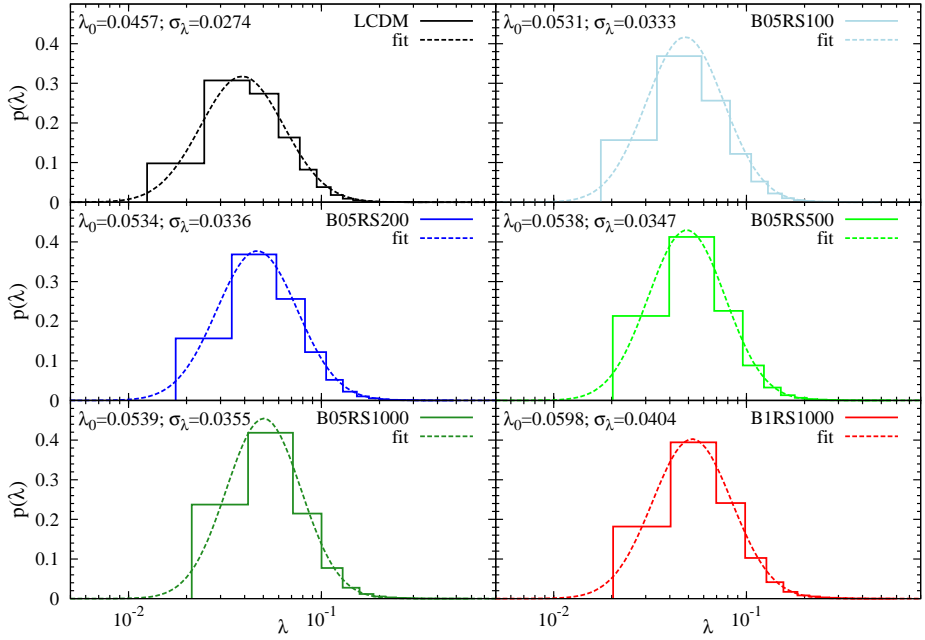


Figure 8. The distributions of the spin parameter accompanied by the fitted log-normal distributions. In each panel we also give the numerically computed mean value and the standard deviation for the distributions.

Table 4. The mean and the standard deviations for the fitted log-normal spin distributions.

Model	λ_0	σ_λ
LCDM	0.0457	0.0274
B05RS100	0.0531	0.0333
B05RS200	0.0534	0.0336
B05RS500	0.0538	0.0347
B05RS1000	0.0539	0.0355
B1RS1000	0.0598	0.0404

seen in the scalar forces cosmologies is not large, it is accompanied by the more dramatic effect of a broadening of the distributions. The increase in σ_λ due to the presence of the scalar forces is much larger than the effect shown for λ_0 and reaches nearly 50% between the Λ CDM and the B1RS1000 cases. Therefore, on average, we can expect to have many more fast rotating haloes in the ReBEL cosmology compared to the fiducial standard LCDM cosmology. This could be a potentially positive effect, as fast rotating DM haloes (high value of the spin parameter) would promote easier spiral think-disk galaxy assembly in such a halo [78, 79].

We will now turn to any (possible) spin-mass dependence. Other authors have established that for N-body simulations of the Λ CDM model the spin depends very weakly on halo mass [80–82]. The observed very small dependence shows that more massive haloes tend to have slightly lower spin parameters. We want to check if this behaviour can also be seen for the ReBEL haloes. We therefore plot the $\lambda - M_{vir}$ distribution in Fig. 9. As usual we plot the 1σ errors only for the LCDM case. Our result for the Λ CDM model agrees with the results of the other authors (e.g. [80, 82]), i.e. we observe a marginal dependence of the from $\lambda \propto M^\alpha$ with the mean slope $\alpha = -0.005$. We can notice nearly the same behaviour for the averaged λ for all our ReBEL models. The average spin is

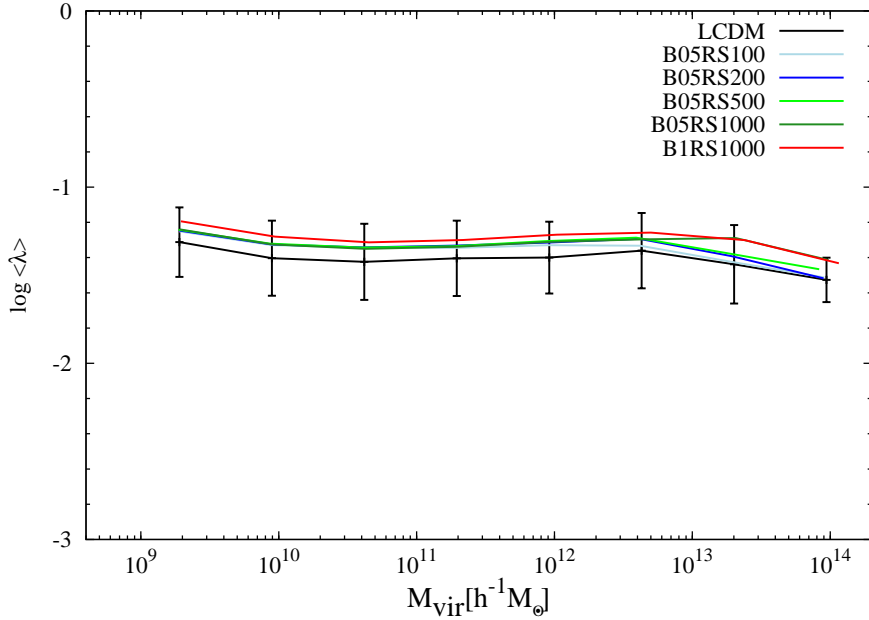


Figure 9. The $\lambda - M_{vir}$ correlation for all our models. For clarity the 1σ errors are plotted only for the Λ CDM case.

of course a bit higher for the models with modified dynamics (as just discussed), but the very weak dependence $\lambda - M_{vir}$ has the same character as for the Λ CDM case. What is interesting to note is that for all ReBEL models – except the models with $r_s = 1000h^{-1}$ kpc – the $\langle \lambda \rangle$ values approach the Λ CDM limit for $M_{vir} > 10^{13}h^{-1}M_\odot$. This is not unexpected when we recall that the virial mass of a halo also corresponds, in fact, to some length scale related to the halo virial radius. Thus we observe here that in terms of an averaged halo spin the bigger the ratio R_{vir}/r_s the less angular momentum it gains due to the presence of the scalar forces. These observations agree with the torque theory of the growth of a halo angular momentum and spin. The scale of the tidal forces shaping the haloes' spins is connected to the length scale set by a given halo's virial radius. Thus for big haloes the enhancement of forces on scales noticeably smaller than its virial radius do not contribute significantly to the process of growth of its angular momentum. Which is exactly what we see in a statistical sense in Fig. 9.

4.3 Shapes and geometry

The shape and the geometry of a halo are determined jointly by linear and non-linear processes. Theoretical predictions are usually constrained to the linear processes influencing the shape of a DM halo. The high complexity characterising the non-linear phenomena acting within a halo makes the prediction of the direct outcome of such processes very difficult. Generally one assumes that three principal factors are responsible for the final halo shape:

- the shape and orientation of the primordial density peak from which the halo originated [83–86],
- the external tidal shear field that shapes the halo [87, 88],
- and the non-linear interactions disturbing the original halo shape, e.g. the violent relaxation and halo merging [89].

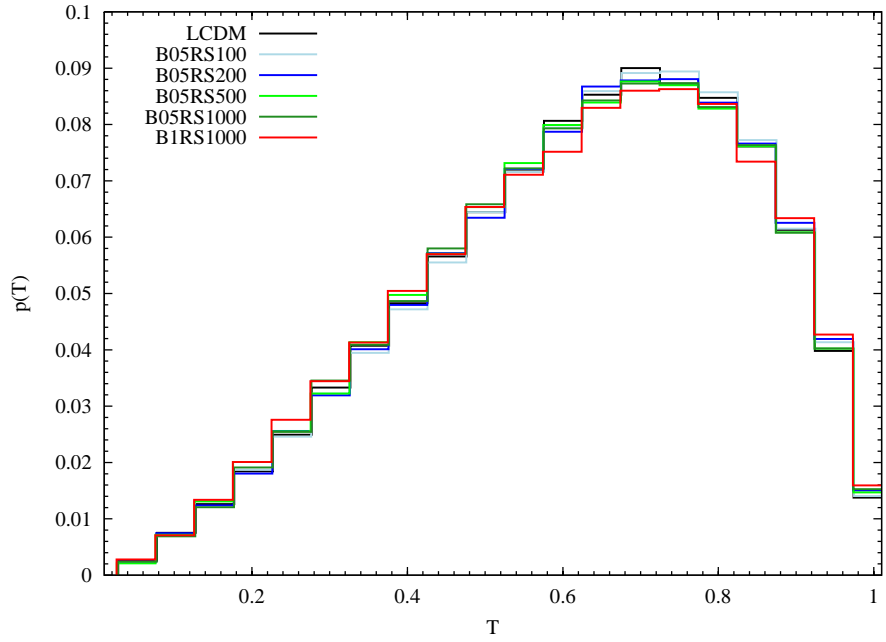


Figure 10. The distributions of the triaxiality parameter T for haloes in our models.

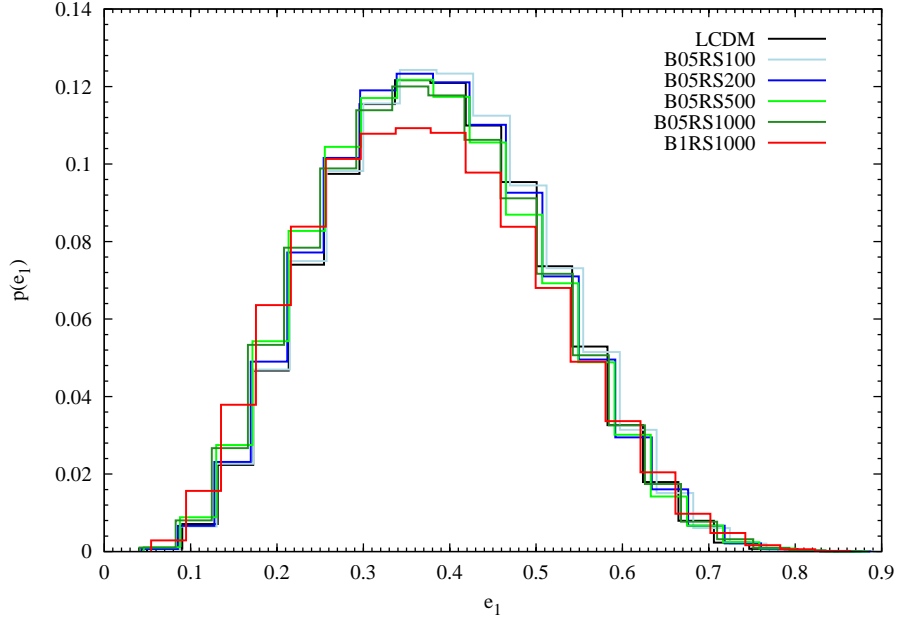


Figure 11. The distributions of the ellipticity parameter e_1 for haloes in our models.

The complex interplay of all above mentioned factors determine the final halo shape and geometry. We now want to check to what extent the presence of the scalar-interactions at the DM particle level will affect the DM halo shapes.

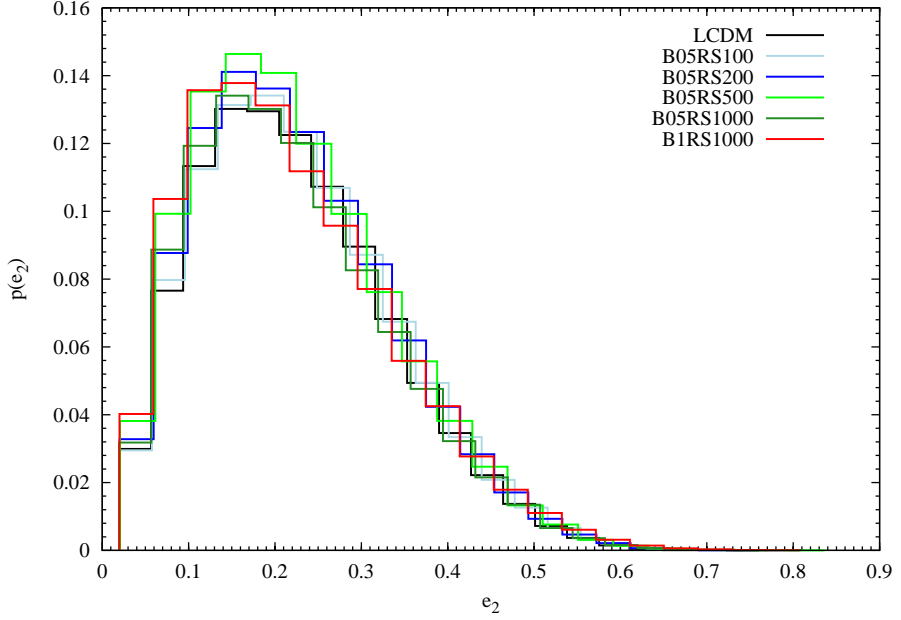


Figure 12. The distributions of the ellipticity parameter e_2 for haloes in our models.

We will determine the halo shape approximating its mass distribution to a triaxial ellipsoid. The halo's axes of inertia can be calculated from the moment of inertia tensor, which we define as:

$$I_{ij} = \sum_i^{N_H} x_i x_j, \quad (4.12)$$

where the particle positions x_i and x_j are ascertain with respect to the centre of the mass of a halo and the sum covers all particles belonging to a given halo. Now one can compute the axes of the ellipsoid using the eigenvectors λ_i of the inertia tensor:

$$\begin{aligned} a &= \sqrt{\lambda_1}, \\ b &= \sqrt{\lambda_2}, \\ c &= \sqrt{\lambda_3}, \end{aligned} \quad (4.13)$$

where

$$a > b > c.$$

As our main measure of the halo shape we use the triaxiality parameter [90]:

$$T = \frac{a^2 - b^2}{a^2 - c^2}. \quad (4.14)$$

High values of the T parameter marks a prolate ellipsoid, while low values of the triaxiality correspond to an oblate halo. We can compute two other parameters related to the triaxiality, namely the ellipticities:

$$e_1 = 1 - \frac{c}{a} \quad \text{and} \quad e_2 = 1 - \frac{b}{a}. \quad (4.15)$$

Table 5. The mean and the standard deviations of the shape parameter distributions for all our models.

Model	$\langle T \rangle$	σ_T	$\langle e_1 \rangle$	σ_{e_1}	$\langle e_2 \rangle$	σ_{e_2}
LCDM	0.6	0.21	0.366	0.122	0.2	0.11
B05RS100	0.6	0.21	0.37	0.124	0.2	0.11
B05RS200	0.6	0.21	0.364	0.124	0.2	0.11
B05RS500	0.598	0.21	0.36	0.126	0.2	0.11
B05RS1000	0.599	0.21	0.359	0.127	0.2	0.11
B1RS1000	0.597	0.21	0.355	0.132	0.2	0.12

The higher the values of these parameters the less spherical the ellipsoid's projection in the planes of the related semi-axis will be.

In Figs. 10, 11 and 12 we present the distributions of the T , e_1 and e_2 parameters, respectively. These distributions were computed using all haloes for a given model. By analysing these figures we reach the conclusion, that the ReBEL forces do not affect the halo shapes in any significant way. We can observe that the distributions of the fiducial model agree quite well with the distributions of modified models. To outline this claim, we have collected in the Tab. 5 the mean values of the parameters alongside their 1σ scatter for all presented distributions. The data from the table indicates that in the statistical sense all inquired distributions agree with each other. The present discrepancies – if any – are no greater than 3%. Thus we can infer that the modified gravity of the from we study in this paper does not reflect itself on the shapes of DM haloes.

4.4 Virialisation

The last, but not least important, question we like to address in this section concerns the stages of the haloes' virialisation in our considered cosmologies. Taking into account all that we already know about the specific features fostered by the ReBEL cosmologies, we should definitely expect significant differences in the stages of virialisation between the Λ CDM and ReBEL halo populations.

As we know, the virialisation is the final stage of the gravitational collapse of a DM halo. During this process the internal energy of the halo is distributed in such way that the halo as an object should attain a perfect equilibrium configuration. Virialisation is very complex and dynamical *modus operandi* of the interplay between gravitation and the physical nature of DM. Usually, if one assumes a simple and idealised spherical model, it is straightforward to get definitive predictions for the virial state and time in an assumed background cosmology. In the real Universe one deals, however, with an array of processes that make precise virial predictions cumbersome. This is due to the fact that a real DM halo is a “living” entity inhabiting the Cosmic Web and thus interacting with its surrounding environment. This is also exacerbated by the fact that non-ideal DM haloes have usually significant amount of substructure as expected in the hierarchical models of CDM. Furthermore, some significant fraction of haloes have shapes that are rather far away from a perfect sphere (as just discussed). This all taken together make the theoretical predictions of the virial states difficult.

Here we now investigate the DM haloes' virialisation in the set of our simulations. Following the virial theorem we can write the virial equation for a self-gravitating system as:

$$\frac{1}{2} \frac{d^2 I}{dt^2} = 2K + U - E_p . \quad (4.16)$$

Here K is the kinetic energy, defined for a halo consisting of total N_H DM particles as:

$$K = \frac{1}{2} \sum_{i=1}^{N_H} m_i u_i^2, \quad (4.17)$$

where m_i is the mass of an i -th particle (for our simulations all particles have equal mass, hence $m_i = m_p$) and u_i is the velocity of an i -th particle with respect to the centre of mass of the halo. Thus u_i is defined as the peculiar velocity of a particle with subtracted bulk velocity of the halo:

$$u_i = v_i - v_{\text{centre}}. \quad (4.18)$$

The potential energy U of the halo in the Newtonian case is given by:

$$U = - \sum_{i=1}^{N_H} \sum_{j=i+1}^{N_H} G \frac{m_p^2}{|\mathbf{r}_i - \mathbf{r}_j|}, \quad (4.19)$$

where the sum of the distances is over all unique particle pairs. When the scalar forces of the ReBEL are present we will have higher potential energies between pairs of particles, thus above formula needs to be adjusted as follows:

$$U^{\text{ReBEL}} = - \sum_{i=1}^{N_H} \sum_{j=i+1}^{N_H} G \frac{m_p^2}{|\mathbf{r}_i - \mathbf{r}_j|} \cdot h(|\mathbf{r}_i - \mathbf{r}_j|), \quad (4.20)$$

where we used the parametrisation of the ReBEL potential enhancement $h(x)$ from (2.19). All effects coming from the environment and surrounding of the halo are encoded in the surface pressure term [91, 92]:

$$E_p = \int P_s(r) \mathbf{r} \cdot d\mathbf{S}. \quad (4.21)$$

We will limit our analysis to the case of an isolated halo, thus we set $E_s = 0$.⁶ The halo is virialised when $\ddot{I} \rightarrow 0$, hence from Eqn. (4.16) we have:

$$2K + U = 0. \quad (4.22)$$

This equation is well known as the Virial Theorem for an idealised and isolated self-gravitating system. Using (4.22) we can define the so-called *virial ratio parameter*, which is a measure of the virial state of an object (for a more detailed and elaborate discussion of measures of a halo's virial state see e.g. [93]):

$$\mathcal{V} = \frac{2K}{|U|}. \quad (4.23)$$

The virial ratio approaches unity for a fully virialised halo, it is in range $1 < \mathcal{V} \leq 2$ for gravitationally bound system and $\mathcal{V} > 2$ depicts an unbound object.

⁶Of course in the real Universe haloes are affected by the distribution of matter in their surroundings and in general the surface pressure terms is not negligible. This term is especially important for more massive haloes (ie. clusters) [92]. However in the following study we will be interested only in the relative difference in the state of virialisation between haloes in our reference Λ CDM model and the different ReBEL runs. We could safely ignore the (4.21) term in our relative comparison, if this terms is influencing the virial state of the haloes in the different models to the same extent. We have computed this term for 10 most massive haloes in our runs and have found that the relative corrections that would arise from including the pressure term are of the same order of magnitude.

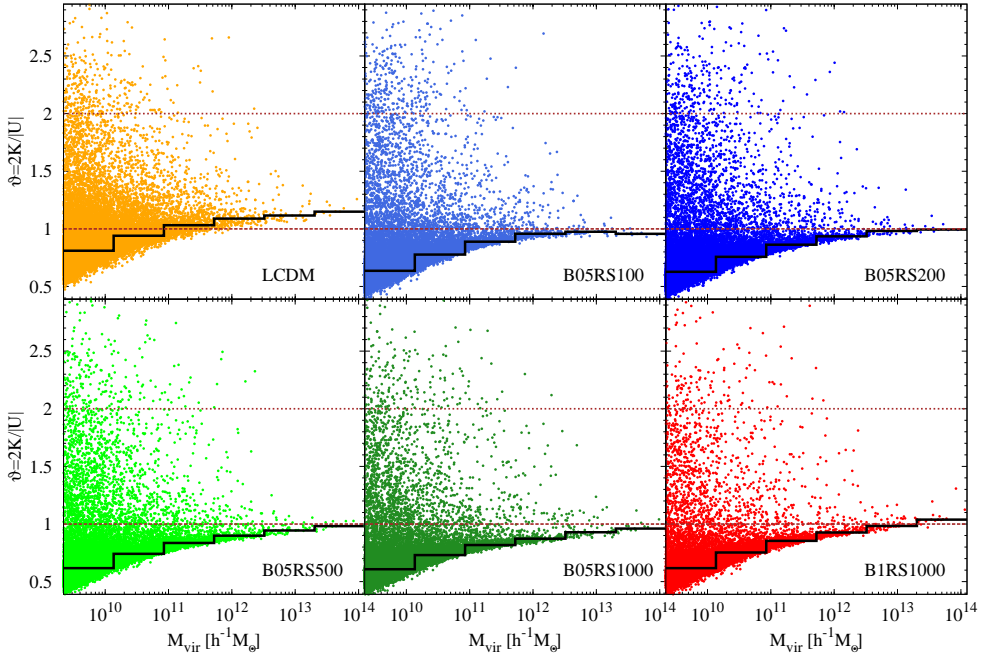


Figure 13. The virial ratios for haloes in all models. Panels show results from the Λ CDM (top-left) to B1RS1000 (bottom-right). In each panel the points show results for individual haloes, where the solid black lines depict the median values computed in mass bins. Horizontal lines mark the virialisation threshold $\mathcal{V} = 1$ (the dashed line) and the gravitational bound threshold $\mathcal{V} = 2$ (the dotted line).

Comparing the Eqs. (4.19) and (4.20) we can expect that for halos with $R_{vir} \ll r_s$ the gravitational energy bounding the halo will increase by factor of $1 + \beta$ thus lowering the virialisation factor. However in the ReBEL model forces that particles exert on each other are also increased providing to some extent higher accelerations thus also higher velocity dispersions. The latter effect will attenuate the former in an overall decrease of the virialisation parameter. Nevertheless we can expect that haloes, on average, will be more virialised in the ReBEL case.

To quantify the latest statement we present Figs. 13 and 14. In the former we plot in six panels the virial ratio as defined by Eqn. (4.23) against the virial halo mass for all our simulation runs. Dots represent the \mathcal{V} values for individual haloes and the solid black lines depict median virial ratio binned in virial halo mass. In each panel we also plot two brown horizontal lines marking the two thresholds for the virial ratio: a virialised state (the dashed line) and gravitationally bounded state (the dotted line). The results shown in the figure clearly underline known effects, e.g. that on average less massive haloes tend to be closer to relaxation and big massive haloes ($M_H \gtrsim 10^{13} - 10^{14} h^{-1} M_\odot$) seem to be somewhat less virialised systems. We can also immediately notice that in all our ReBEL runs the majority of DM haloes have lower values of the virial state \mathcal{V} than haloes in the fiducial Λ CDM run. It is clearly visible when looking at the lines depicting averaged virial ratios binned in halo mass. To study this effect in more detail we show in Fig. 14 only median virial ratios (top panel) accompanied by the plot of relative deviations of this quantity from the Λ CDM case $\Delta\mathcal{V} = \mathcal{V}_{ReBEL}/\mathcal{V}_{LCDM}$ (the bottom panel). Undoubtedly the ReBEL haloes, on average, are more virialised than their LCDM cousins.

The effect is especially prominent for low-mass haloes. On the other hand we also see that this “enhanced virialisation” effect present in the ReBEL runs depends weakly on the scalar interaction model parameters. There is a visible weak trend for the virial mass in the range $10^{11} h^{-1} M_\odot \lesssim$

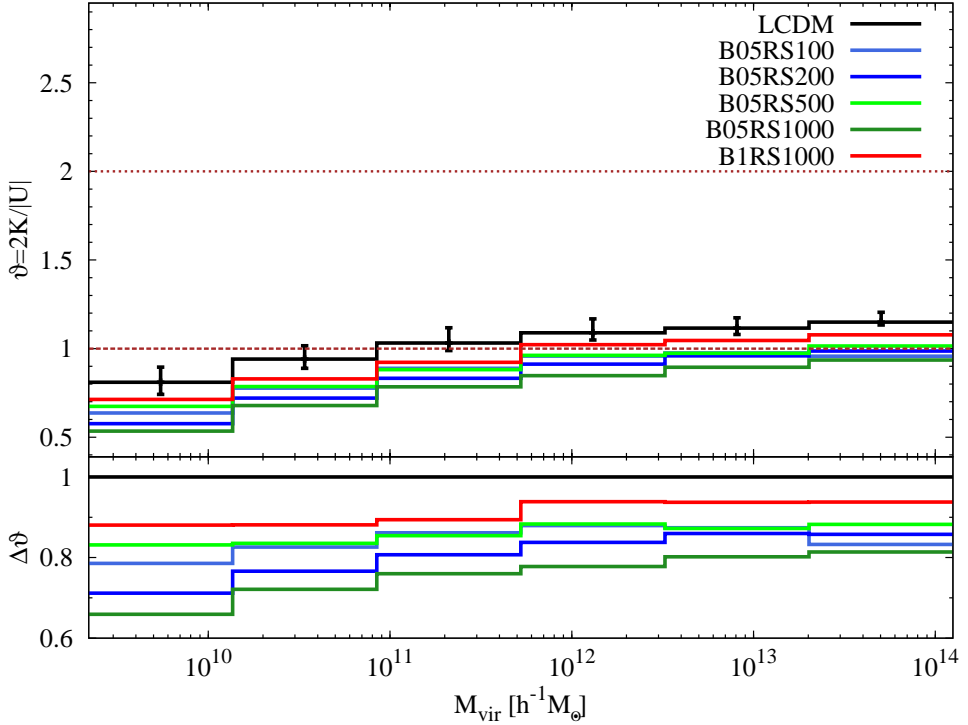


Figure 14. Top panel: the median virial ratios for all models binned in halo mass. For clarity we plot the errorbars only for the Λ CDM case, they represent the upper and lower quartiles of the sample. Bottom panel: The deviation of mass-binned virial ratios from the LCDM case $\Delta\mathcal{V} = \mathcal{V}_{ReBEL}/\mathcal{V}_{LCDM}$ for the ReBEL models haloes.

$M_{vir} \lesssim 10^{13}h^{-1}M_\odot$, where the models with the same value of $\beta = 0.5$ but with different screening lengths r_s show more impact on the value of $\Delta\mathcal{V}$. Namely the bigger the value of r_s the more virialisation we get for bigger haloes. This is to be expected, because as we have discussed already, the virial mass of a halo corresponds also to a specific scale - the virial radius of this halo. Thus again the effect of the scalar forces here is, to some extent, depended on the value of the R_{vir}/r_s ratio. The situation is quite different when we consider the strongest ReBEL model tested in the B1RS1000 run. Here we observe that for masses $M_{vir} \gtrsim 10^{11}h^{-1}M_\odot$ the effect of the scalar forces on the averaged \mathcal{V} values is actually weaker than in models B05RS500 and B05RS1000. For the very few most massive haloes that we could identify in our runs with $M_{vir} \gtrsim 10^{13}h^{-1}M_\odot$ the imprint on the \mathcal{V} made by the B1RS1000 model is even smaller than that made by the two of our models with the smallest screening lengths (B05RS100 & B05RS200). We can explain this at first sight unexpected result, if we recall that in the ReBEL cosmologies when one considers the virialisation process of a DM halo, one should remember that the scalar interactions increase not only the binding potential energy of the halo but they also increase the accelerations of the DM particles. Thus in the ReBEL picture, the scalar forces increase also to some extent the summary kinetic energy of a given halo. As we stated earlier, this effect attenuates partially the increase of the halo binding energy. Hence it seems that our study here has shown that this attenuation is significantly increased for the $\beta = 1$ case. If we compare directly the curves in the lower panel of the Fig. 14 marking the B05RS1000 and B1RS1000 models we see that for the same value of the screening length $r_s = 1000h^{-1}$ kpc the amplitude of the deviation factor $\Delta\mathcal{V}$ differs significantly between the models for $M_{vir} \gtrsim 10^{11}h^{-1}m_\odot$. Even when we take into account that for the $\beta = 1$ case the effect of the "fifth force" on the virial ratio is a

bit smaller for more massive haloes, we can undoubtedly assert that on average for all our *ReBEL* models DM haloes are more virialised with respect to the haloes from the fiducial Λ CDM run.

5 Results: Properties of cross-correlated haloes

We will now investigate the dependence of individual halo properties on the *ReBEL* cosmology parameters. To this extent we perform a cross-correlation of particles in identified objects between the different *ReBEL* runs and – taken as the reference – the Λ CDM run.

We employ a tool included in the distribution of the AHF halo finder, which establishes for two given halo catalogues – for this purpose consisting of the particle IDs – for each halo from the first catalogue the best matching halo from the second catalogue. This is done by maximising the quantity

$$\xi = \frac{N_{\text{shared}}^2}{N_1 N_2} \quad (5.1)$$

where N_{shared} is the number of shared particles between two haloes and N_1 and N_2 are the total number of particles in the halo from the first and the second catalogue, respectively. As the different models use the same phases when generating the initial conditions we should be able to cross-correlate the different simulations, finding for each halo of the Λ CDM model its corresponding halo in each of the *ReBEL* runs. In addition to the condition of maximising the merit function Eq. 5.1 we also require that the connection is unique, i.e. we require that every halo appears only once in the final cross-correlated list. Matching the Λ CDM haloes with their *ReBEL* twins can be unsuccessful for some cases. Especially when considering haloes containing less and less particles, finding a unique cross-correlation becomes more and more difficult. To overcome that problem we constrain our cross-correlations to those Λ CDM haloes containing at least 10^4 particles, thus for haloes with $M_{\text{vir}} \geq 2.03 \times 10^{11} h^{-1} M_\odot$. By applying this constrain we assure that for all our Λ CDM haloes we could find unique matching twins from the *ReBEL* runs.

We will now study imprints and direct effects of the *ReBEL* forces exerted on DM haloes comparing various internal properties of objects cross-correlated between cosmologies twins.

5.1 The virial mass

We begin with comparing the quantity that is most severely affected by the presence of the scalar interactions in the DM sector. This is – of course – the final virial mass of a DM halo as we have seen earlier. We already know that in the *ReBEL* cosmology haloes form earlier as violent merging and relaxation processes are taking place at earlier cosmic epochs compared to the fiducial Λ CDM model [11]. More effective (hierarchical) structure formation must result in higher final masses of the majority of haloes. This is exactly the effect we can infer from Fig. 15, where we plot the mass ratio ($M_{\text{ReBEL}}/M_{\Lambda\text{CDM}}$) of the cross-correlated pairs against the virial mass of the referenced Λ CDM halo $M_{\Lambda\text{CDM}}$. In each panel we plot results for individual cross-correlated pairs (dots) as well as median ratios binned in Λ CDM halo mass (solid lines) accompanied by the errorbars marking the first and third quartile of the values in each bin. In the last bottom-right panel we plot again median trends for all models to allow for an easier cross-model data comparison. We will follow this convention from now on for all figures in this section. First we denote that individual halo pair ratios have a rather large scatter and this scatter grows as we move to *ReBEL* models with stronger scalar interactions. However, if we look at the median ratio we clearly see that the net effect of the scalar interaction is that the majority of DM haloes arrive at $z = 0$ carrying more mass w.r.t. their Λ CDM cousins and, moreover, the value of this net effect depends on the *ReBEL* model parameters. The larger the screening length and/or strength parameter the more increase of final halo mass we measure. Just

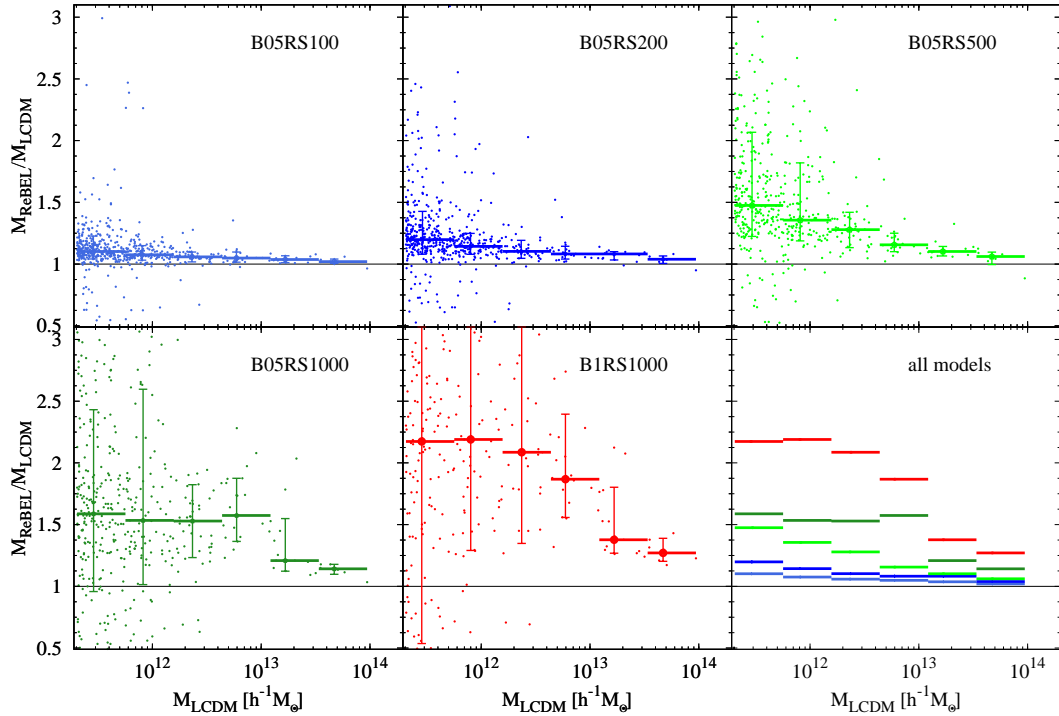


Figure 15. Comparison of the cross-correlated halo masses in all considered models. The solid lines depict median values, while the errorbars mark the upper and lower quartiles.

like in the case of the virial parameter here we observe again that the less massive given halo is the more it is affected by the scalar forces. The mass excess noted for the ReBEL cross-correlated haloes quickly decreases as we move towards masses corresponding to galaxy groups and clusters ($M_{vir} \gtrsim 10^{13} - 10^{14} h^{-1} M_\odot$). For our models with the shortest screening lengths $r_s = 100, 200 h^{-1}$ kpc this mass range is barely affected with the median excess being smaller than a few per cent. Only for the models with the largest screening length $r_s = 1 h^{-1}$ Mpc this mass range shows a more significant excess of the order of 20 – 30%. This effect is, in principle, unobservable; however, it can be potentially interesting in the light of the recent reports of massive clusters and superclusters found at intermediate redshifts $z \gtrsim 1$ [28–30]. Many authors claim that these observations pose a challenge to theoretical predictions of structure formation in Λ CDM and some class of Dynamical Dark Energy models [31–33]. In our models with $\beta = 0.5, 1.0$ and $r_s = 500, 1000 h^{-1}$ kpc the observed net mass excess for the most massive haloes found in our simulations could help to accommodate massive clusters and superclusters seen in recent observations. Here we discussed this mass excess effect only briefly, but to see if the ReBEL forces could really alleviate the tension a more comprehensive study is needed. This was already pointed out to some extend in previous studies of the ReBEL model halo mass functions [9, 11].

5.2 The triaxiality parameter

Now we will compare the cross-correlated halo triaxiality parameters as defined by Eqn. (4.14). As previously discussed in Sec. 4.3 we did not notice (in general) any significant effect of the scalar forces on the triaxiality distributions. This is also confirmed by plots of cross-correlated T_{ReBEL}/T_{LCDM} ratios shown in Fig. 16. Despite the quite large scatter for individual halo pairs the net effect of the scalar interactions as seen in the median mass-binned ratio is marginal. We can

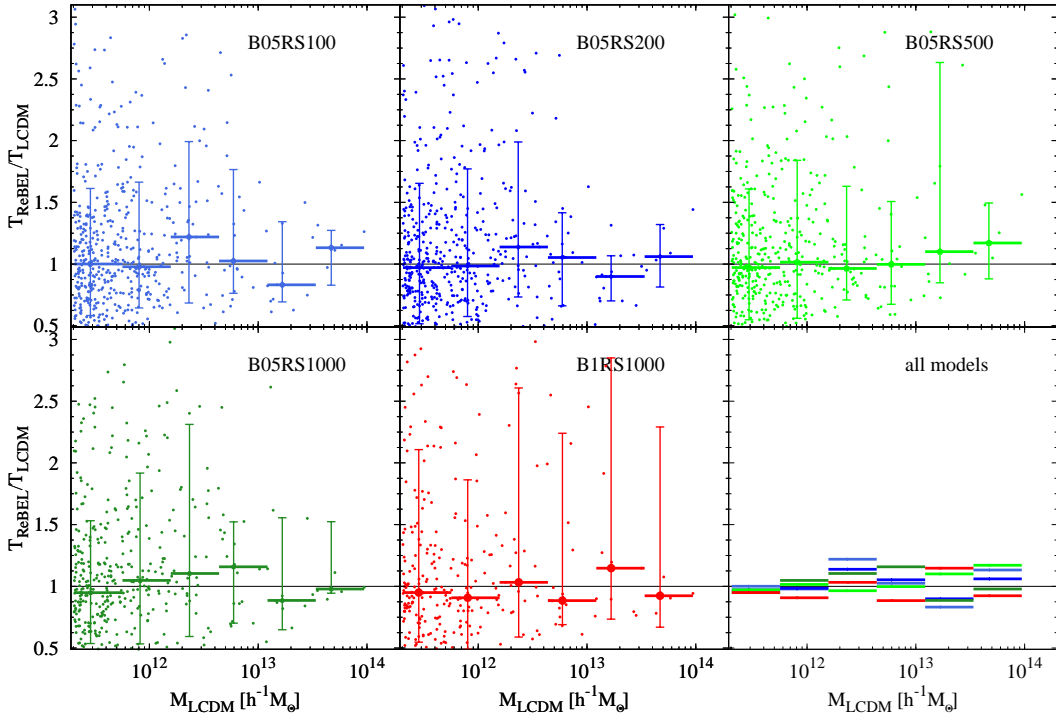


Figure 16. Comparison of the cross-correlated halo triaxiality parameter. The meanings of lines is identical to Fig. 15.

conclude again that the presence of the scalar forces in the DM sector does not, on average, effect the final halo shape.

5.3 The spin parameter

In this subsection we will focus on the direct comparison of the halo-halo spin parameter ratio between the Λ CDM and the ReBEL runs. In Fig. 17 we plot again six panels depicting the $\lambda_{ReBEL}/\lambda_{LCDM}$ ratios for cross-correlated pairs of haloes together with the median ratio. Looking at the individual panels of that figure we see that the overall effect is small for all models except the B1RS1000 where for the mass bin $1.5 \times 10^{12} h^{-1} M_\odot \leq M_{LCDM} \leq 3.5 \times 10^{12} h^{-1} M_\odot$ we observe a peculiar strong peak in the median spin ratio. We inspected that feature closely and have found that this unusual peak is a manifestation of the smallness of our data sample in that mass range. Because we are dealing with small number statistics here we are severely affected by random fluctuations. In that mass bin there are 35 cross-correlated haloes for that model and 8 of those haloes have a $\lambda_{ReBEL}/\lambda_{LCDM}$ ratio higher than 3. To conclude, we can say that the increase of the spin parameter of the ReBEL haloes' counter-partners depends on the considered halo mass and on the values of the ReBEL model parameters. Generally we see that the effect is more pronounced for low mass haloes and also the median increase of the spin ratio is higher for models with higher screening lengths. This result agrees with our previous considerations about the statistically averaged spin parameter for the halo populations presented in section 4.2.

5.4 The concentrations

Finally for the last comparison in this section we chose the ratio of the cross-correlated haloes virial concentration parameter defined by Eqn. (4.2). We plot the corresponding results in Fig. 18. Here

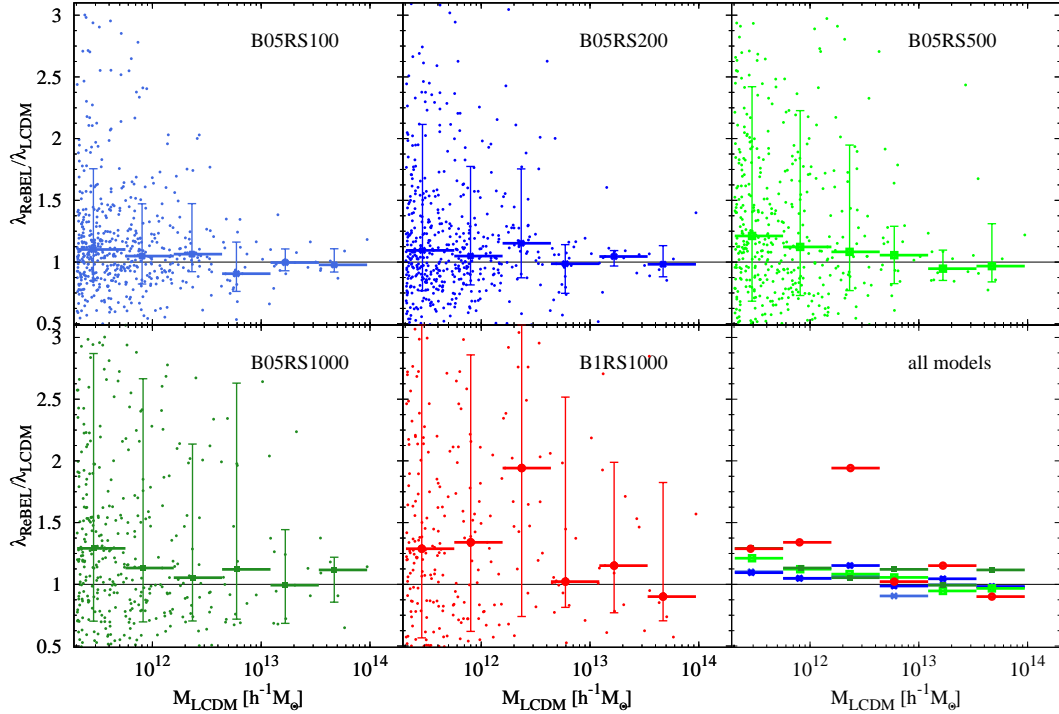


Figure 17. Comparison of the cross-correlated halo spin parameter. The meanings of lines is identical to Fig. 15.

we can denote a very interesting effect confirming again our previous statistical study. Namely, the most prominent effect of the concentration parameter increase (ignoring the B1RS1000 model for the moment) can be seen for the two ReBEL models with the shortest screening lengths – B05RS100 and B05RS200. Moreover, the concentration increase seems to be halo mass dependent, being larger for higher masses. The overall effect is strongest for the B1RS1000 model cross-correlated pairs. However, this is not surprising, if we take into account that this model has two times stronger scalar forces than the rest of the inquired models. Nevertheless it is very interesting to note that the effect of increased concentration parameter seems weakest in the two intermediate ReBEL models: B05RS500 and B05RS1000. What is also important is the fact that this effect is much more pronounced for the galaxy group and clusters like haloes and is only of $10 \sim 15\%$ for Milky-Way mass like haloes with $M \sim 10^{12} h^{-1} M_\odot$. This seems to be not too bad news for the ReBEL cosmology since if the increase in the concentration parameter at the $M^{12} M_\odot$ mass scale would be more severe it would promote for the ReBEL haloes even worse 'cusp' problem than we have for the fiducial Λ CDM model haloes. The increase of the scalar-interacting DM haloes virial concentration parameter with respect to their Λ CDM cousins reflects earlier formation times of the ReBEL haloes reported in [11].

6 Conclusions

In this paper we have studied averaged and cross-correlated internal properties of Dark Matter haloes in a cosmological scenario invoking exotic physics in the Dark Matter sector. The new physics considered here involves long-range fifth-forces in the DM inducing the weak equivalence principle breaking and modified dynamics of the pressureless DM fluid at scales below 1 Mpc. To this end we have conducted a series of N-body simulations of inquired models altogether with our fiducial Λ CDM

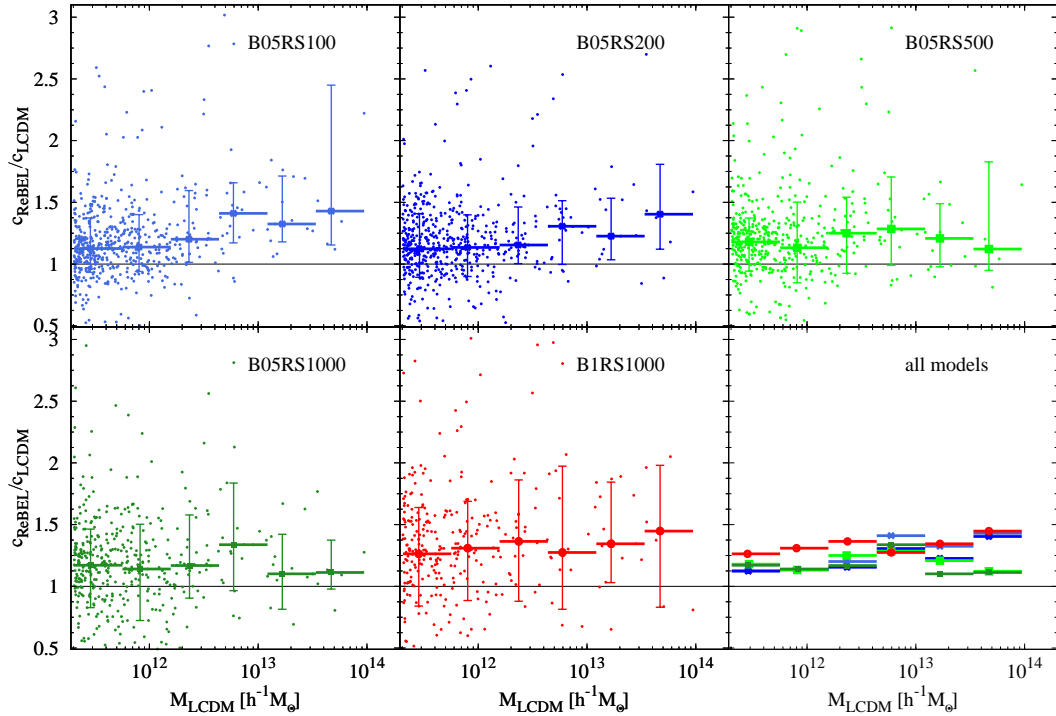


Figure 18. Comparison of the cross-correlated halo concentration parameter. The meaning of the lines is the same as in Fig. 15.

model starting from the same initial conditions: the initial density perturbations power spectrum and Fourier components phases. Using the phenomenological approximation of the scalar-interacting DM model by means of the modified Newtonian gravity we have assured that our N-body and halo finding codes are properly including modified physics. In our analysis we have found and described many interesting effects that appear when one deals with the halo (and structure) formation in modified gravity regime. We can summarise our findings in the following list:

- We have denoted that despite modified gravity is acting between DM particles the resulting haloes, on average, are still well described by a universal DM halo density profile – the NFW profile [60]. We have found, however, that on average the density profiles of the ReBEL haloes are characterised by higher virial concentrations when compared with the density profiles of Λ CDM haloes. However, this effect is not large, reaching from $\sim 6\%$ on average up to $\sim 15\%$ for the B1RS1000 model.
- The averaged rotation curves of all models agree within 1σ scatter in the four virial radius/mass ranges used for stacking. However, we noted a systematic shift of r_{max} towards smaller values for the ReBEL haloes. This effect, however, that is statistical not significant for our particular halo data sample, agrees with the increase of the virial concentrations noted for averaged and cross-correlated haloes.
- The analysis of the haloes' spin parameter distributions has revealed that the ReBEL haloes are characterised by a higher mean spin λ_0 and standard deviations values. This indicated that in a statistical sense the DM haloes in the inquired modified cosmologies have higher rotational support, thus they spin faster. We confirmed also that within the framework of the ReBEL

cosmology the $\lambda - M_{vir}$ relation is of the same shape and character like for the Λ CDM haloes: on average the more massive haloes are marginally less rotationally supported.

- Our studies have further shown that the modified gravity of the scalar-interacting DM does not change the geometry and shapes of the haloes. The distributions of the both elliptisities as well as the triaxiality parameter are in statistical agreement for Λ CDM and ReBEL haloes. This implies that the initial conditions have much more effect on the final halo shapes than a particular form of their dynamical evolution (e.g. a form of the force-law).
- The scalar interactions considered in this work rise the potential energy of DM particles residing inside the halo potential wells. Thanks to this the general degree of virialisation of ReBEL haloes is higher than in the Λ CDM case. We have shown this by using the virial ratio $\mathcal{V} = \frac{2K}{|U|}$ as the measure of a halo's virial state. This effect was denoted for haloes in all mass ranges considered in our simulations.
- The analysis of the direct halo-halo cross-correlations between the Λ CDM and ReBEL haloes has generally confirmed the findings from the statistical analysis. One interesting remark to make here is that in the case of halo virial concentration parameter c_{vir} the cross-correlation revealed that for the majority of tested ReBEL flavours the net effect of increased concentration is much more pronounced for high mass haloes. Thus in principle the galaxy-mass haloes' density profiles are much less affected by the scalar forces than concentrations of density profiles of galaxy-group and cluster mass DM haloes.

Our findings here taken together, surprisingly, do not form a strong observable prospects for DM haloes as probes of modified gravity. The form of modified gravity employed in our studies was only a phenomenological formulation of an underlying exotic DM physics including dynamically screened scalar interactions. Nevertheless effectively we modelled DM halo formation and non-linear evolution in the regime of modified gravity. Our studies have shown that DM haloes appear to be rather non-susceptible to gravity effectively enhanced at scales below one megaparsec. We have found some imprints in the density profiles (higher virial concentrations) as well as in the distribution of the spin parameter, but the deviations from the values typical for the genuine Λ CDM haloes are rather small. This implies that statistically the ReBEL DM haloes are not so different from their Λ CDM cousins. This opens the window for the ReBEL model to reproduce the successes of Λ CDM-based galaxy formation theories, producing at the same time interesting features in the spatial clustering patterns (e.g. more empty cosmic voids [1, 9] or faster formation of non-linear structures [11]) that make the ReBEL structure formation scenarios significantly different from the standard paradigm. This work focused on theoretical studies concerning internal properties of DM haloes in modified cosmological scenarios. The ultimate challenge for the ReBEL theory will be to pass the observational tests. This calls for a successful employment of the ReBEL model physics with relativistic galaxy formation modelling. We leave this challenging task for a future study.

Acknowledgments

The authors want to thanks Alexander Merson for carefully reading this manuscript. Some of the simulations used in this research was performed on the `halo2` cluster at the Interdisciplinary Center for Mathematical and computational Modelling of the University of Warsaw. WAH would like to acknowledge the hospitality of the Institute of Astronomy at the University of Zielona Góra that he has received during his stay there. WAH also acknowledge the support of this research received from Polish National Science Center in grant no. DEC-2011/01/D/ST9/01960. SRK acknowledges support

by the Ministerio de Ciencia e Innovacion (MICINN) under the Consolider-Ingenio, SyeC project CSD-2007-00050. AK acknowledges support by the Spanish Ministerio de Ciencia e Innovacion (MICINN) in Spain through the Ramon y Cajal programme as well as the grants AYA 2009-13875-C03-02, AYA2009-12792-C03-03, CSD2009-00064, and CAM S2009/ESP-1496. He also thanks Burt Bacharach for alfie.

References

- [1] J. A. Keselman, A. Nusser, and P. J. E. Peebles, *Cosmology with equivalence principle breaking in the dark sector*, *Phys. Rev. D* **81** (Mar., 2010) 063521, [[arXiv:0912.4177](https://arxiv.org/abs/0912.4177)].
- [2] P. J. E. Peebles and A. Nusser, *Nearby galaxies as pointers to a better theory of cosmic evolution*, *Nature* **465** (June, 2010) 565–569, [[arXiv:1001.1484](https://arxiv.org/abs/1001.1484)].
- [3] P. J. E. Peebles, *The Void Phenomenon*, *Astrophys. J.* **557** (Aug., 2001) 495–504, [[astro-ph/](https://arxiv.org/abs/astro-ph/)].
- [4] S. S. Gubser and P. J. E. Peebles, *Structure formation in a string-inspired modification of the cold dark matter model*, *Phys. Rev. D* **70** (Dec., 2004) 123510, [[hep-th/04](https://arxiv.org/abs/hep-th/04)].
- [5] S. S. Gubser and P. J. E. Peebles, *Cosmology with a dynamically screened scalar interaction in the dark sector*, *Phys. Rev. D* **70** (Dec., 2004) 123511, [[hep-th/04](https://arxiv.org/abs/hep-th/04)].
- [6] G. R. Farrar and P. J. E. Peebles, *Interacting Dark Matter and Dark Energy*, *Astrophys. J.* **604** (Mar., 2004) 1–11, [[astro-ph/0307316](https://arxiv.org/abs/astro-ph/0307316)].
- [7] G. R. Farrar and R. A. Rosen, *A New Force in the Dark Sector?*, *Phys. Rev. Lett.* **98** (Apr., 2007) 171302, [[astro-ph/0610298](https://arxiv.org/abs/astro-ph/0610298)].
- [8] A. Nusser, S. S. Gubser, and P. J. Peebles, *Structure formation with a long-range scalar dark matter interaction*, *Phys. Rev. D* **71** (Apr., 2005) 083505, [[astro-ph/0412586](https://arxiv.org/abs/astro-ph/0412586)].
- [9] W. A. Hellwing and R. Juszkiewicz, *Dark matter gravitational clustering with a long-range scalar interaction*, *Phys. Rev. D* **80** (Oct., 2009) 083522, [[arXiv:0809.1976](https://arxiv.org/abs/0809.1976)].
- [10] W. A. Hellwing, *Galactic halos in cosmology with long-range scalar DM interaction*, *Annalen der Physik* **19** (2010), no. 3-5 351–354, [[arXiv:0911.0573](https://arxiv.org/abs/0911.0573)].
- [11] W. A. Hellwing, S. R. Knollmann, and A. Knebe, *Boosting hierarchical structure formation with scalar-interacting dark matter*, *MNRAS* **408** (Oct., 2010) L104–L108, [[arXiv:1004.2929](https://arxiv.org/abs/1004.2929)].
- [12] R. Cen, *Cosmological reionization in LCDM models with and without a scalar field*, *New Astronomy Review* **50** (Mar., 2006) 191–198.
- [13] W. A. Hellwing, R. Juszkiewicz, and R. van de Weygaert, *Hierarchy of N-point functions in the Λ CDM and ReBEL cosmologies*, *Phys. Rev. D* **82** (Nov., 2010) 103536, [[arXiv:1008.3930](https://arxiv.org/abs/1008.3930)].
- [14] M. Baldi, V. Pettorino, G. Robbers, and V. Springel, *Hydrodynamical N-body simulations of coupled dark energy cosmologies*, *MNRAS* **403** (Apr., 2010) 1684–1702, [[arXiv:0812.3901](https://arxiv.org/abs/0812.3901)].
- [15] M. Baldi, *Simulations of structure formation in interacting dark energy cosmologies*, *Nuclear Physics B Proceedings Supplements* **194** (Oct., 2009) 178–184, [[arXiv:0906.5353](https://arxiv.org/abs/0906.5353)].
- [16] B. Li and J. D. Barrow, *On the effects of coupled scalar fields on structure formation*, *MNRAS* **413** (May, 2011) 262–270, [[arXiv:1010.3748](https://arxiv.org/abs/1010.3748)].
- [17] B. Li, *Voids in coupled scalar field cosmology*, *MNRAS* **411** (Mar., 2011) 2615–2627, [[arXiv:1009.1406](https://arxiv.org/abs/1009.1406)].
- [18] B. Li, D. F. Mota, and J. D. Barrow, *N-body Simulations for Extended Quintessence Models*, *ApJ* **728** (Feb., 2011) 109, [[arXiv:1009.1400](https://arxiv.org/abs/1009.1400)].
- [19] B. Li and J. D. Barrow, *N-body simulations for coupled scalar-field cosmology*, *Phys. Rev. D* **83** (Jan., 2011) 024007, [[arXiv:1005.4231](https://arxiv.org/abs/1005.4231)].

[20] M. Baldi, *Clarifying the effects of interacting dark energy on linear and non-linear structure formation processes*, *MNRAS* **414** (June, 2011) 116–128, [[arXiv:1012.0002](https://arxiv.org/abs/1012.0002)].

[21] M. Baldi, *Time-dependent couplings in the dark sector: from background evolution to non-linear structure formation*, *MNRAS* **411** (Feb., 2011) 1077–1103, [[arXiv:1005.2188](https://arxiv.org/abs/1005.2188)].

[22] A.-C. Davis, B. Li, D. F. Mota, and H. A. Winther, *Structure Formation in the Symmetron Model*, *ArXiv e-prints* (Aug., 2011) [[arXiv:1108.3081](https://arxiv.org/abs/1108.3081)].

[23] M. Baldi, *Early massive clusters and the bouncing coupled dark energy*, *ArXiv e-prints* (July, 2011) [[arXiv:1107.5049](https://arxiv.org/abs/1107.5049)].

[24] M. Baldi, J. Lee, and A. V. Macciò, *The Effect of Coupled Dark Energy on the Alignment Between Dark Matter and Galaxy Distributions in Clusters*, *ApJ* **732** (May, 2011) 112, [[arXiv:1101.5761](https://arxiv.org/abs/1101.5761)].

[25] B. Li and H. Zhao, *Structure formation by the fifth force: Segregation of baryons and dark matter*, *Phys. Rev. D* **81** (May, 2010) 104047, [[arXiv:1001.3152](https://arxiv.org/abs/1001.3152)].

[26] H. Zhao, A. V. Macciò, B. Li, H. Hoekstra, and M. Feix, *Structure Formation by Fifth Force: Power Spectrum from N-Body Simulations*, *ApJ* **712** (Apr., 2010) L179–L183, [[arXiv:0910.3207](https://arxiv.org/abs/0910.3207)].

[27] H. Shan, B. Qin, B. Fort, C. Tao, X.-P. Wu, and H. Zhao, *Offset between dark matter and ordinary matter: evidence from a sample of 38 lensing clusters of galaxies*, *MNRAS* **406** (Aug., 2010) 1134–1139, [[arXiv:1004.1475](https://arxiv.org/abs/1004.1475)].

[28] A. M. Swinbank and et al., *The discovery of a massive supercluster at $z = 0.9$ in the UKIDSS Deep eXtragalactic Survey*, *MNRAS* **379** (Aug., 2007) 1343–1351, [[arXiv:0706.0090](https://arxiv.org/abs/0706.0090)].

[29] R. J. Foley, K. Andersson, G. Bazin, T. de Haan, J. Ruel, P. A. R. Ade, K. A. Aird, R. Armstrong, M. L. N. Ashby, M. Bautz, B. A. Benson, L. E. Bleem, M. Bonamente, M. Brodwin, J. E. Carlstrom, C. L. Chang, A. Clocchiatti, T. M. Crawford, A. T. Crites, S. Desai, M. A. Dobbs, J. P. Dudley, G. G. Fazio, W. R. Forman, G. Garmire, E. M. George, M. D. Gladders, A. H. Gonzalez, N. W. Halverson, F. W. High, G. P. Holder, W. L. Holzapfel, S. Hoover, J. D. Hrubes, C. Jones, M. Joy, R. Keisler, L. Knox, A. T. Lee, E. M. Leitch, M. Lueker, D. Luong-Van, D. P. Marrone, J. J. McMahon, J. Mehl, S. S. Meyer, J. J. Mohr, T. E. Montroy, S. S. Murray, S. Padin, T. Plagge, C. Pryke, C. L. Reichardt, A. Rest, J. E. Ruhl, B. R. Saliwanchik, A. Saro, K. K. Schaffer, L. Shaw, E. Shirokoff, J. Song, H. G. Spieler, B. Stalder, S. A. Stanford, Z. Staniszewski, A. A. Stark, K. Story, C. W. Stubbs, K. Vanderlinde, J. D. Vieira, A. Vikhlinin, R. Williamson, and A. Zenteno, *Discovery and Cosmological Implications of SPT-CL J2106-5844, the Most Massive Known Cluster at $z \approx 1$* , *ApJ* **731** (Apr., 2011) 86, [[arXiv:1101.1286](https://arxiv.org/abs/1101.1286)].

[30] M. Brodwin, J. Ruel, P. A. R. Ade, K. A. Aird, K. Andersson, M. L. N. Ashby, M. Bautz, G. Bazin, B. A. Benson, L. E. Bleem, J. E. Carlstrom, C. L. Chang, T. M. Crawford, A. T. Crites, T. de Haan, S. Desai, M. A. Dobbs, J. P. Dudley, G. G. Fazio, R. J. Foley, W. R. Forman, G. Garmire, E. M. George, M. D. Gladders, A. H. Gonzalez, N. W. Halverson, F. W. High, G. P. Holder, W. L. Holzapfel, J. D. Hrubes, C. Jones, M. Joy, R. Keisler, L. Knox, A. T. Lee, E. M. Leitch, M. Lueker, D. P. Marrone, J. J. McMahon, J. Mehl, S. S. Meyer, J. J. Mohr, T. E. Montroy, S. S. Murray, S. Padin, T. Plagge, C. Pryke, C. L. Reichardt, A. Rest, J. E. Ruhl, K. K. Schaffer, L. Shaw, E. Shirokoff, J. Song, H. G. Spieler, B. Stalder, S. A. Stanford, Z. Staniszewski, A. A. Stark, C. W. Stubbs, K. Vanderlinde, J. D. Vieira, A. Vikhlinin, R. Williamson, Y. Yang, O. Zahn, and A. Zenteno, *SPT-CL J0546-5345: A Massive $z \approx 1$ Galaxy Cluster Selected Via the Sunyaev-Zel'dovich Effect with the South Pole Telescope*, *ApJ* **721** (Sept., 2010) 90–97, [[arXiv:1006.5639](https://arxiv.org/abs/1006.5639)].

[31] E. Carlesi, A. Knebe, G. Yepes, S. Gottloeber, J. Beltran Jimenez, and A. L. Maroto, *Vector dark energy and high- z massive clusters*, *ArXiv e-prints* (Aug., 2011) [[arXiv:1108.4173](https://arxiv.org/abs/1108.4173)].

[32] M. Baldi and V. Pettorino, *High- z massive clusters as a test for dynamical coupled dark energy*, *MNRAS* **412** (Mar., 2011) L1–L5, [[arXiv:1006.3761](https://arxiv.org/abs/1006.3761)].

[33] M. J. Mortonson, W. Hu, and D. Huterer, *Simultaneous falsification of Λ CDM and quintessence with massive, distant clusters*, *Phys. Rev. D* **83** (Jan., 2011) 023015, [[arXiv:1011.0004](https://arxiv.org/abs/1011.0004)].

[34] G. Nordström, *Zur Theorie der Gravitation vom Standpunkt des Relativitätsprinzips*, *Annalen der Physik* **347** (1913) 533–554.

[35] H. Yukawa, *On the Interaction of Elementary Particles*, *Proceedings of the Physico-Mathematical Society of Japan* **17** (1935) 48–57.

[36] R. H. Dicke, *Scalar-Tensor Gravitation and the Cosmic Fireball*, *ApJ* **152** (Apr., 1968) 1.

[37] R. H. Dicke, *Long-Range Scalar Interaction*, *Physical Review* **126** (June, 1962) 1875–1877.

[38] P. Jordan, *Zum gegenwärtigen Stand der Diracschen kosmologischen Hypothesen*, *Zeitschrift für Physik* **157** (Feb., 1959) 112–121.

[39] T. Damour, G. W. Gibbons, and C. Gundlach, *Dark matter, time-varying G , and a dilaton field*, *Physical Review Letters* **64** (Jan., 1990) 123–126.

[40] B.-A. Gradwohl and J. A. Frieman, *Dark matter, long-range forces, and large-scale structure*, *Astrophys. J.* **398** (Oct., 1992) 407–424.

[41] J. A. Frieman and B.-A. Gradwohl, *Dark matter and the equivalence principle*, *Physical Review Letters* **67** (Nov., 1991) 2926–2929.

[42] J. A. Casas, J. García-Bellido, and M. Quiros, *Scalar-tensor theories of gravity with Φ -dependent masses*, *Classical and Quantum Gravity* **9** (May, 1992) 1371–1384, [[hep-ph/92](#)].

[43] T. Damour and A. M. Polyakov, *String theory and gravity*, *General Relativity and Gravitation* **26** (Dec., 1994) 1171–1176, [[gr-qc/941](#)].

[44] C. Wetterich, *An asymptotically vanishing time-dependent cosmological "constant"*., *A&A* **301** (Sept., 1995) 321, [[hep-th/94](#)].

[45] G. W. Anderson and S. M. Carroll, *Dark Matter with Time-Dependent Mass*, in *COSMO-97, First International Workshop on Particle Physics and the Early Universe* (L. Roszkowski, ed.), p. 227, 1998.

[46] R. Bean, *Perturbation evolution with a nonminimally coupled scalar field*, *Phys. Rev. D* **64** (Dec., 2001) 123516, [[astro-ph/0104464](#)].

[47] L. Amendola, *Perturbations in a coupled scalar field cosmology*, *MNRAS* **312** (Mar., 2000) 521–530, [[astro-ph/9906073](#)].

[48] L. Amendola and D. Tocchini-Valentini, *Baryon bias and structure formation in an accelerating universe*, *Phys. Rev. D* **66** (Aug., 2002) 043528, [[astro-ph/0111535](#)].

[49] U. França and R. Rosenfeld, *Fine Tuning in Quintessence Models with Exponential Potentials*, *Journal of High Energy Physics* **10** (Oct., 2002) 15, [[astro-ph/0206194](#)].

[50] T. Damour, F. Piazza, and G. Veneziano, *Violations of the equivalence principle in a dilaton-runaway scenario*, *Phys. Rev. D* **66** (Aug., 2002) 046007, [[hep-th/02](#)].

[51] D. Comelli, M. Pietroni, and A. Riotto, *Dark energy and dark matter*, *Physics Letters B* **571** (Oct., 2003) 115–120, [[hep-ph/03](#)].

[52] L. Amendola, M. Gasperini, and F. Piazza, *Fitting type Ia supernovae with coupled dark energy*, *Journal of Cosmology and Astro-Particle Physics* **9** (Sept., 2004) 14, [[astro-ph/0407573](#)].

[53] P. J. E. Peebles, *The large-scale structure of the universe*. Research supported by the National Science Foundation. Princeton, N.J., Princeton University Press, 1980. 435 p., 1980.

[54] V. Springel, *The cosmological simulation code GADGET-2*, *MNRAS* **364** (Dec., 2005) 1105–1134, [[astro-ph/0505010](#)].

[55] S. P. D. Gill, A. Knebe, and B. K. Gibson, *The evolution of substructure - I. A new identification method*, *MNRAS* **351** (June, 2004) 399–409, [[astro-ph/0404258](#)].

[56] S. R. Knollmann and A. Knebe, *AHF: Amiga's Halo Finder*, *ApJS* **182** (June, 2009) 608–624, [[arXiv:0904.3662](#)].

[57] W. E. Schaap and R. van de Weygaert, *Continuous fields and discrete samples: reconstruction through Delaunay tessellations*, [A&A 363](#) (Nov., 2000) L29–L32, [[astro-ph/0011007](#)].

[58] F. Bernardeau and R. van de Weygaert, *A new method for accurate estimation of velocity field statistics*, [MNRAS 279](#) (Mar., 1996) 693.

[59] M. C. Cautun and R. van de Weygaert, *The DTFe public software - The Delaunay Tessellation Field Estimator code*, [ArXiv e-prints](#) (May, 2011) [[arXiv:1105.0370](#)].

[60] J. F. Navarro, C. S. Frenk, and S. D. M. White, *A Universal Density Profile from Hierarchical Clustering*, [ApJ 490](#) (Dec., 1997) 493, [[astro-ph/9611107](#)].

[61] F. Hoyle, *The Origin of the Rotations of the Galaxies*, in [Problems of Cosmical Aerodynamics](#), p. 195, 1951.

[62] P. J. E. Peebles, *Origin of the Angular Momentum of Galaxies*, [ApJ 155](#) (Feb., 1969) 393.

[63] A. G. Doroshkevich, *The space structure of perturbations and the origin of rotation of galaxies in the theory of fluctuation*, [Astrofizika 6](#) (1970) 581–600.

[64] G. Efstathiou and B. J. T. Jones, *The rotation of galaxies - Numerical investigations of the tidal torque theory*, [MNRAS 186](#) (Jan., 1979) 133–144.

[65] S. M. Fall and G. Efstathiou, *Formation and rotation of disc galaxies with haloes*, [MNRAS 193](#) (Oct., 1980) 189–206.

[66] S. D. M. White, *Angular momentum growth in protogalaxies*, [ApJ 286](#) (Nov., 1984) 38–41.

[67] P. J. E. Peebles, *Origin of the Angular Momentum of Galaxies*, [ApJ 155](#) (Feb., 1969) 393.

[68] M. Vitvitska, A. A. Klypin, A. V. Kravtsov, R. H. Wechsler, J. R. Primack, and J. S. Bullock, *The Origin of Angular Momentum in Dark Matter Halos*, [ApJ 581](#) (Dec., 2002) 799–809, [[astro-ph/](#)].

[69] J. Barnes and G. Efstathiou, *Angular momentum from tidal torques*, [ApJ 319](#) (Aug., 1987) 575–600.

[70] M. S. Warren, P. J. Quinn, J. K. Salmon, and W. H. Zurek, *Dark halos formed via dissipationless collapse. I - Shapes and alignment of angular momentum*, [ApJ 399](#) (Nov., 1992) 405–425.

[71] B. Robertson, J. S. Bullock, T. J. Cox, T. Di Matteo, L. Hernquist, V. Springel, and N. Yoshida, *A Merger-driven Scenario for Cosmological Disk Galaxy Formation*, [ApJ 645](#) (July, 2006) 986–1000, [[astro-ph/](#)].

[72] J. S. Bullock, A. Dekel, T. S. Kolatt, A. V. Kravtsov, A. A. Klypin, C. Porciani, and J. R. Primack, *A Universal Angular Momentum Profile for Galactic Halos*, [Astrophys. J. 555](#) (July, 2001) 240–257, [[astro-ph/0011001](#)].

[73] M. S. Warren, P. J. Quinn, J. K. Salmon, and W. H. Zurek, *Dark halos formed via dissipationless collapse. I - Shapes and alignment of angular momentum*, [ApJ 399](#) (Nov., 1992) 405–425.

[74] S. Cole and C. Lacey, *The structure of dark matter haloes in hierarchical clustering models*, [MNRAS 281](#) (July, 1996) 716, [[astro-ph/9510147](#)].

[75] H. J. Mo, S. Mao, and S. D. M. White, *The formation of galactic discs*, [MNRAS 295](#) (Apr., 1998) 319–336, [[astro-ph/9707093](#)].

[76] M. Steinmetz and M. Bartelmann, *On the spin parameter of dark-matter haloes*, [MNRAS 272](#) (Feb., 1995) 570–578, [[astro-ph/9403017](#)].

[77] P. Catelan and T. Theuns, *Evolution of the angular momentum of protogalaxies from tidal torques: Zel'dovich approximation*, [MNRAS 282](#) (Sept., 1996) 436–454, [[astro-ph/9604077](#)].

[78] F. Governato, B. Willman, L. Mayer, A. Brooks, G. Stinson, O. Valenzuela, J. Wadsley, and T. Quinn, *Forming disc galaxies in Λ CDM simulations*, [MNRAS 374](#) (Feb., 2007) 1479–1494, [[astro-ph/0602351](#)].

[79] B. Robertson, J. S. Bullock, T. J. Cox, T. Di Matteo, L. Hernquist, V. Springel, and N. Yoshida, *A*

Merger-driven Scenario for Cosmological Disk Galaxy Formation, [ApJ 645](#) (July, 2006) 986–1000, [[astro-ph/0503369](#)].

- [80] A. V. Macciò, A. A. Dutton, F. C. van den Bosch, B. Moore, D. Potter, and J. Stadel, *Concentration, spin and shape of dark matter haloes: scatter and the dependence on mass and environment*, [MNRAS 378](#) (June, 2007) 55–71, [[astro-ph/0608157](#)].
- [81] P. Bett, V. Eke, C. S. Frenk, A. Jenkins, J. Helly, and J. Navarro, *The spin and shape of dark matter haloes in the Millennium simulation of a Λ cold dark matter universe*, [MNRAS 376](#) (Mar., 2007) 215–232, [[astro-ph/0608607](#)].
- [82] A. Knebe and C. Power, *On the Correlation between Spin Parameter and Halo Mass*, [ApJ 678](#) (May, 2008) 621–626, [[arXiv:0801.4453](#)].
- [83] J. M. Bardeen, J. R. Bond, N. Kaiser, and A. S. Szalay, *The statistics of peaks of Gaussian random fields*, [ApJ 304](#) (May, 1986) 15–61.
- [84] J. R. Bond and S. T. Myers, *The Peak-Patch Picture of Cosmic Catalogs. I. Algorithms*, [ApJS 103](#) (Mar., 1996) 1.
- [85] R. van de Weygaert and E. Bertschinger, *Peak and gravity constraints in Gaussian primordial density fields: An application of the Hoffman-Ribak method*, [MNRAS 281](#) (July, 1996) 84, [[astro-ph/9507024](#)].
- [86] R. K. Sheth, H. J. Mo, and G. Tormen, *Ellipsoidal collapse and an improved model for the number and spatial distribution of dark matter haloes*, [MNRAS 323](#) (May, 2001) 1–12, [[astro-ph/9907024](#)].
- [87] J. R. Bond, L. Kofman, and D. Pogosyan, *How filaments of galaxies are woven into the cosmic web*, [Nature 380](#) (Apr., 1996) 603–606, [[astro-ph/9512141](#)].
- [88] R. van de Weygaert, *Clusters and the Cosmic Web*, [ArXiv Astrophysics e-prints](#) (July, 2006) [[astro-ph/0607539](#)].
- [89] M. van Haarlem and R. van de Weygaert, *Velocity Fields and Alignments of Clusters in Gravitational Instability Scenarios*, [ApJ 418](#) (Dec., 1993) 544.
- [90] M. Franx, G. Illingworth, and T. de Zeeuw, *The ordered nature of elliptical galaxies - Implications for their intrinsic angular momenta and shapes*, [ApJ 383](#) (Dec., 1991) 112–134.
- [91] S. Chandrasekhar, *Hydrodynamic and hydromagnetic stability*. 1961.
- [92] L. D. Shaw, J. Weller, J. P. Ostriker, and P. Bode, *Statistics of Physical Properties of Dark Matter Clusters*, [ApJ 646](#) (Aug., 2006) 815–833, [[astro-ph/](#)].
- [93] C. Power, A. Knebe, and S. R. Knollmann, *The dynamical state of dark matter haloes in cosmological simulations - I. Correlations with mass assembly history*, [MNRAS](#) (Oct., 2011) 1734, [[arXiv:1109.2671](#)].